Optical, chemical properties and oxidative potential of aqueous-phase products from OH and ^{3}C*-initiated photolysis of eugenol

Xudong Li[1], Ye Tao[1], Longwei Zhu[1], Shuaishuai Ma[1], Shipeng Luo[1], Zhuzi Zhao[1], Ning Sun[1], Xinlei Ge[2,*], Zhaolian Ye[1,*]

[1]College of Chemistry and Environmental Engineering, Jiangsu University of Technology, Changzhou 213001, China

[2]Jiangsu Key Laboratory of Atmospheric Environment Monitoring and Pollution Control, Collaborative Innovation Center of Atmospheric Environment and Equipment Technology, School of Environmental Sciences and Engineering, Nanjing University of Information Science and Technology, Nanjing 210044, China

*Correspondence: Zhaolian Ye (bess_ye@jsut.edu.cn) and Xinlei Ge (caxinra@163.com)

Abstract: Aqueous reactions may turn precursors into more light-absorbing and toxic products, leading to air quality deterioration and adverse health effects, etc. In this study, we investigated comprehensively eugenol degradationphotooxidation (a representative biomass burning emitted, highly substituted phenolic compound) in thebulk aqueous phase bywith direct photolysis, hydroxyl radical (OH) and indirect photooxidation in the presence of radicals (an organic triplet excited state (^{3}C*) and hydroxyl radical (•OH)).*). Results showed show that the degradation rates of eugenol followed the order of ^{3}C*>•OH >direct photolysis. Relative contributions of reactive oxygen species (ROS) were evaluated via combination of radical quenching tests, deoxygenatedQuenching experiments and electron spin resonance (ESR) method, and results showed verified that ^{3}C* indeed played a dominant role in eugenol degradation for ^{3}C*-initiated

26 oxidation, while $O_2^{\bullet-}$–generated ~~were~~was important for OH-initiated oxidation.

27 ~~Rate~~Photolysis rate constants under saturated O_2, air and N_2 followed the order of k_{O_2}

28 $> k_{Air} > k_{N_2}$ for both direct photolysis and OH-initiated oxidation, ~~and it~~but changed to

29 $k_{Air} > k_{N_2} > k_{O_2}$ for $^3C^*$-~~initiated~~mediated oxidation. pH and dissolved oxygen (DO)

30 levels both decreased during oxidation, indicating formation of acids and the

31 participation of DO in oxidation. UV-vis light absorption spectra of the reaction

32 products showed clear absorbance enhancement in the 300-400 nm range ~~after~~

33 ~~photooxidation,~~for all three cases and new ~~fluorescent spectra~~fluorescence at

34 excitation/emission=250~~/~~(400-500) nm appeared, suggesting the formation of new

35 chromophores and fluorophores~~, such as~~ (brown carbon species); and these species

36 were likely attributed to humic-like substances (HULIS~~). Concentration~~) as shown by

37 the increases of ~~generated~~ HULIS ~~first increased gradually then leveled off over time.~~

38 ~~Dithiothreitol~~concentrations during oxidation. Large mass yields of products (140%-

39 197%) after 23 hours of illumination were obtained, and high oxidation degrees of these

40 products were also observed; correspondingly, a series of oxygenated compounds were

41 identified, and detailed reaction mechanism with functionalization as a dominant

42 pathway was proposed. At last, dithiothreitol (DTT) assay was applied to assess

43 oxidation potential of ~~products, which was greater~~the reaction products, and the end

44 products in all three photolysis conditions showed higher DDT consumption rates than

45 that of ~~eugenol, suggesting~~the precursor, indicating more ~~harmful~~toxic species were

46 produced ~~during oxidation. The carbon oxidation state and oxygen to carbon ratio~~

47 ~~from~~upon aqueous oxidation. Overall, our results by using eugenol as a model

48 compound, underscore the potential importance of aqueous processing of biomass

49 burning emissions in secondary organic aerosol ~~mass spectrometry both increased with~~

50 ~~time, indicating that~~ (SOA ~~became more oxidized. Detailed reaction pathways were~~

2

elucidated via analyses of chemical characteristics of the products) formation, as well as its impacts on particulate matter concentration and toxicity, radiative balance and climate change.

1 Introduction

Photochemical reactions in atmospheric aqueous ~~phase~~phases (cloud ~~droplet, /~~fog ~~droplet~~droplets and aerosol water) can affect ~~the~~ lifetimes of many organic species, and are ~~an~~ important ~~sources~~source and ~~aging~~ pathway of secondary organic aerosol (SOA) formation (Vione et al., 2006; Zhao et al., 2012). ~~Different from~~Compared to the gas~~SOA~~ formed ~~through~~via gas-phase photochemical oxidation, aqueous-phase SOA (aqSOA) ~~typically~~ is ~~usually~~often more oxidized and less volatile, ~~so it plays~~therefore might play an important role in haze formation, air quality and global climate change (Ervens et al., 2011; Lim et al., 2010). However, due to complexity of ~~reaction mechanisms~~the aqueous reactions and ~~control~~influencing factors (such as precursors, oxidants, and light ~~source), there are still many unknowns regarding aqueous reactions. For example,~~intensities), detailed reaction mechanism, optical property, oxidative potential (OP) and ~~relations between~~the interplay among them remain poorly understood.

~~Most~~Many laboratory studies ~~so far~~ have focused on aqueous-phase ~~oxidation~~oxidations of ~~small~~low molecular weight (LMW) volatile organic compounds (VOCs~~,~~), such as isoprene, terpenes (α~~-pinene and~~-, β-pinene), as well as their gas-phase oxidation products (such as glyoxal, methylglyoxal, *cis*-pinonic acid and methyl vinyl ketone) (Faust et al., 2017; Herrmann, 2003; Herrmann et al., 2015; Huang et al., 2011; Lee et al., 2012; Zhang et al., 2010). ~~Now concerns have been extended to~~Recently, aqueous oxidation of semi-/intermediate volatility VOCs (S/IVOCs),

76 ~~especially~~such as the phenolic compounds~~, which could be produced by~~ emitted from

77 combustion or pyrolysis of lignin in biomass, were also extensively investigated

78 (Barzaghi and Herrmann, 2002; Bonin et al., 2007; Chen et al., 2020; Gilardoni et al.,

79 2016; He et al., 2019; Jiang et al., 2021; Li et al., 2014; Li et al, 2021; Ma et al., 2021;

80 Mabato et al., 2022; Smith et al., 2014; Sun et al., 2010; Tang et al., 2020; Yang et al.,

81 2021; Yu et al., 2016). Generally, chemical ~~structure~~structures of precursors ~~has~~have

82 profound ~~influence~~influences on ~~aqSOA and~~the reaction mechanisms~~, however, the~~

83 and products, while effect of ~~oxidant on SOA formation~~oxidants also cannot be

84 neglected. It is evident that liquid water ~~contains many~~can contain various types of

85 oxidants, such as singlet oxygen ($^1O_2$), nitrate radical (NO_3), hydroxyl radical ($\bullet$OH),

86 and organic triplet excited states ($^3C^*$), ~~which~~and all can play crucial roles in

87 ~~photochemical oxidation~~photooxidation reactions (Kaur and Anastasio, 2018; Scharko

88 et al., 2014). Among them, $\bullet$OH is ~~the~~a ubiquitous oxidant ~~in atmospheric condensed~~

89 ~~phase,~~with ~~concentration~~concentrations of 10^{-13}-10^{-12} mol·L^{-1} (Arakaki et al., 2013;

90 Gligorovski et al., 2015; Herrmann et al., 2003). Hence, aqueous ~~phase~~ $\bullet$OH-induced

91 ~~photodegradation~~photooxidation has been extensively studied (Chen et al., 2020; Sun

92 et al., 2010; Yu et al., 2016). Compared to $\bullet$OH oxidation, $^3C^*$-initiated aqueous ~~phase~~

93 ~~reaction~~ oxidation (photosensitized reaction) has also attracted ~~attention~~attentions in

94 recent years (Ma et al., 2021; Wang et al., 2021). Several classes of organic compounds

95 in ~~the atmosphere~~ambient air, including non-phenolic aromatic carbonyls, quinones,

96 aromatic ketones and nitrogen-containing heterocyclic compounds, can form $^3C^*$ after

97 absorbing light (Alegría et al., 1999; Kaur et al., 2019; Nau and Scaiano, 1996;

98 Rossignol et al., 2014~~).~~; Chen et al., 2018). These compounds are termed as

99 photosensitizers. $^3C^*$ is capable of reacting with O_2 to produce singlet oxygen ($^1O_2$) and

100 superoxide radicals ($O_2^{\bullet-}$). Various reactive oxygen species (ROS) can be generated and

play a critical role in~~ ~~affect greatly the $^3C^*$-initiated aqueous-phase reactions. Despite ~~strong evidence in support of the~~some studies demonstrating importance of ROS in photochemical process (Ma et al, 2021;Wang et al., 2020; Wang et al., 2021; Wu et al., 2021), ~~however,~~ our current understanding on $^3C^*$-initiated ~~SOA~~oxidation is still limited.

Excitation–~~ ~~emission matrix (EEM) ~~fluorescent~~fluorescence spectroscopy, as a low-cost, rapid, non-destructive and high-sensitivity technique, can offer detailed information on chromophores hence has been widely employed for studies of aquatic dissolved organic matter (Aryal et al., 2015). Nevertheless, it has not been extensively used in atmospheric aerosol research (Mladenov et al., 2011). ~~Several recent~~Prior studies have investigated the relationship between the fluorescence components and chemical structures of atmospheric aerosols ~~through combining~~by using high-resolution aerosol mass spectrometry (AMS) and EEM ~~fluorescent~~fluorescence spectroscopy (Chen et al., 2016a; Chen et al., 2016b). ~~Earlier~~An earlier report from Chang and Thompson (2010) found fluorescence spectra of aqueous-phase reaction products ~~during aqueous reaction~~ of phenolic compounds, ~~with~~had some similarities with ~~fluorescence characteristics~~those of humic-like substances (HULIS~~). Subsequently, numerous studies have observed light-absorbing products formed in aqueous photodegradation~~), and ~~further verified~~Tang et al. (2020) reported that aqueous ~~reaction was~~photooxidation of vanillic acid could be a potential source of HULIS ~~(Li et al., 2021; Smith et al., 2016; Tang et al., 2020). Recently, Li et al. (2021) began to apply EEM technique to characterize formation of light-absorbing compounds in aqueous phase oxidation of syringic acid. Additionally, studies (~~. Chang and Thompson,~~ ~~ (2010) also showed that light-absorbing and fluorescent substances generally ~~have~~had large conjugated moieties (i.e., quinones, HULIS, polycyclic aromatic hydrocarbons (PAHs)),

126 which can damage human body (Dou et al., 2015; McWhinney et al., 2013). HULIS

127 are considered as an important contributor to induce oxidative stress since they can

128 serve as electron carriers to catalyze ROS formation (Dou et al., 2015; Ma et al., 2019;

129 Huo et al., 2021; Xu et al., 2020), causing adverse health ~~effect~~effects. Dithiothreitol

130 (DTT) assay (Alam et al., 2013~~; Chen et al., 2021~~; Verma et al., 2015a), as a non-cellular

131 method, was widely employed to determine oxidation activity and ~~assess oxidative~~

132 ~~potential~~OP of atmospheric PM ~~via the rate of DTT consumption~~ (Chen et al., 2019;

133 Cho et al., 2005~~), since oxidative stress was related to adverse~~) for the evaluation of its

134 health ~~effect~~effects. Some other works (Fang et al., 2016; McWhinney et al., 2013;

135 Verma et al., 2015; Zhang et al., 2022) focused on the link between chemical

136 composition and OP in PM, and ~~have~~ confirmed that several kinds of compounds, such

137 as quinones, HULIS and transition metals usually ~~have~~had strong DTT activities.

138 However, ~~to the best of our knowledge,~~ DTT method ~~has not been applied~~is rarely used

139 to evaluate the OP of aqueous-phase oxidation products ~~up to now.~~previously (Ou et al.,

140 2021).

141   In the present work, we ~~choose 4-allyguaiacol/~~chose eugenol~~,~~ (ally guaiacol) as a

142 model compound to conduct aqueous ~~phase reaction.~~oxidation experiment. As a

143 representative methoxyphenol emitted from biomass burning (BB) (Hawthorne et al.,

144 1989; Simpson et al., 2005), it was widely detected in atmospheric particles. For

145 instance, ~~emission~~ concentration and emission factor ~~emitted~~of this compound from

146 beech ~~stove~~wood burning were 0.032 μg/m^3 and 1.534 μg/g, which ~~are~~were twice ~~of~~

147 those of guaiacol (0.016 μg/m^3 and 0.762 μg/g) ~~guaiacol~~ (Bari et al., 2009~~; Liu et al.,~~

148 ~~2019).~~). Eugenol is a ~~representative~~ semivolatile aromatic ~~compounds~~compound with

149 a moderate water-solubility (2.46 g/L at 298 K~~).~~

150   ~~The~~) too. Chemical characteristics of aqueous reaction products ~~were~~

statistically under direct photolysis (without oxidant) and oxidations by OH and $^3C^*$ radicals, were comprehensively elucidated by combining results from a suite of analytical techniques including high-performance liquid chromatography (HPLC), ultraviolet and visible (UV-Vis) spectrophotometry, gas chromatography mass spectrometry (GC-MS), EEM and soot particle aerosol mass spectrometer spectrometry (SP-AMS). The relative importance of various ROS species to eugenol degradation was explored in order to clarify reaction mechanism. This study also investigated the. Moreover, light absorption, fluorescent and oxidative properties of the aqueous oxidation products. Comparison on product properties under direct photolysis (without oxidant) and oxidation by •OH and $^3C^*$ were carried out also investigated.

2 Materials and methods

2.1 Chemicals and reagents

Eugenol (99%), tert-butanol (TBA, 99%), 3,4-dimethoxybenzaldehyde (DMB, 99%), para-benzoquinone (p-BQ, 99%), dithiothreitol (99%) and 5,5′-dithiobis-2-nitrobenzoic acid (DTNB, 99%), 2-nitro-5-thiobenzoic (99%) and %), 5,5-dimethyl-1-pyrroline N-oxide (DMPO), 2,2,6,6-tetramethylpiperidine (TEMP) were all purchased from Sigma-Aldrich chemical company.. Superoxide dismutase (SOD) was purchased from Bovine Erythrocytes BioChemika. Dichloromethane (HPLC-MS grade, 99%), methanol (HPLC-MS grade, 99%), acetonitrile (HPLC-MS grade, 98%), hydrogen peroxide (H_2O_2 (, 35 wt. %), and 2,4,6-trimethylphenol (TMP, 99%) were all obtained from Acors Chemicals. Sodium azide (NaN_3, 98%) was purchased from J&K Scientific Ltd. (Beijing, China). All solutions were prepared using ultrapure water (Millipore) on

174 the ~~day~~days of experiments.

<comment>带格式的: 字体: 加粗

2.2 Photochemical ~~experiment~~oxidation experiments

176   Aqueous—-phase photochemical reactions were carried out in a Rayonet
177 photoreactor (model RPR-200~~),~~) equipped with 16 light tubes (~~equipped with~~ 2 RPR-
178 3000, 7 RPR-3500 and 7 RPR-4190 tubes), which was frequently used to mimic
179 sunlight for photochemical ~~reaction~~experiments and was described in ~~detail~~details by
180 several groups (George et al., 2015; Hong et al., 2015; Huang et al., 2018; Jiang et al.,
181 2021; Zhao et al., 2014~~) to mimic sunlight.~~). Pyrex tubes containing sample
182 ~~solution~~solutions were placed in the ~~central~~center and received radiation from
183 surrounded lamps ~~from~~of all sides. To ensure mixing of the solution, a fan and a
184 magnetic stir bar ~~are~~were placed at ~~the~~ bottom of ~~solution.~~the reaction tube. The
185 solution temperature was controlled at $25\pm2°C$. The same photoreactor system ~~was the~~
186 ~~same as above mentioned~~ and a normalized distribution of ~~the~~ photon fluxes inside
187 ~~RPR-200 illumination system~~the reactor have been reported elsewhere (George et al.,
188 2015~~). According to previous description, the~~), and the wavelength of ~~photon~~
189 ~~fluxes~~light was ~~over~~in the range of 280~~and~~~500 nm~~range. In this work, we~~. We only
190 measured light intensity at ~~the~~ surface of the ~~reaction~~ solution with a radiometer
191 (Photoelectric instrument factory of Everfine Corporation, Hangzhou, China~~). The light~~
192 ~~intensity~~), which was determined to be ~2400 $\mu W/cm^2$ in the range of 290-320 nm

带格式的: 上标

193 (UVB~~) was ·2400 µW/cm², which was~~), lower than the sunlight intensity (6257.1
194 $\mu W/cm^2$).
195   In this work, 300 μM H_2O_2 and 15 μM DMB were added into ~~solution~~solutions as
196 sources of ·OH and $^3C^*$ radicals, respectively. The initial ~~concentrations~~concentration
197 of eugenol was ~~applied as~~ 300 μM. For $^3C^*$-mediated ~~experiment~~experiments, solutions

8

were adjusted to pH=3 by sulfuric acid in order to perform experiments under optimal conditions (Ma et al., 2021; Smith et al., 2014) since DMB triplet state is protonated to a more reactive form in acidic ~~solutions~~solution. We conducted three sets of photolysis experiments: (A) 300 µM eugenol~~+~~ + 300 µM H_2O_2~~;~~, (B) 300 µM eugenol~~+~~ + 15 µM DMB~~;~~, and (C) 300 µM eugenol~~.~~ without oxidants. In each series of ~~photochemical oxidation~~experiments, a dark control ~~experiments~~experiment was ~~done~~performed synchronously with a Pyrex ~~tubes~~tube wrapped by the aluminum foil. ~~The control results~~Results showed ~~the~~loss of eugenol under dark ~~reaction could be~~conditions were negligible (data not shown). In addition, to evaluate the ~~role~~roles of ROS ~~to~~in eugenol degradation ~~in~~during $^3C^*$-initiated oxidation~~ process~~, quenching experiments by using specific scavengers to ~~trapping produced~~capture different ROS were performed, ~~such as~~namely TBA for ·OH, NaN_3 for $^1O_2$, SOD for $O_2^{·-}$, and TMP for $^3C^*$, respectively (Pan et al., 2020; Wu et al., 2021). ~~In ·~~For OH-initiated oxidation~~ process~~, quenching experiments using p-BQ for $O_2^{·-}$ (Ma et al., 2019; Raja et al., 2005), and TBA for ·OH were conducted. For most ~~series of~~experiments, ~~solution was~~solutions were saturated by air and ~~all experiments~~each experiment presented ~~were conducted in triplicate~~was repeated three times unless otherwise stated. ~~The~~Average results ~~were shown in respect of average plus/minus~~with one standard deviation~~.~~ were provided. In order to further evaluate the role of oxygen in ~~the photodegradation, experiment~~ <mark>photooxidation, experiments</mark> were also conducted ~~under~~by using different saturated ~~gas~~gases (air, N_2 and O_2).

2.3 Analytical methods

2.3.1 Determination of eugenol ~~concentration~~concentrations

Before and during the photochemical ~~reaction~~experiment, 2 mL of reacted ~~and~~
9

222 ~~controlled solutions were~~solution was sampled periodically and subjected to HPLC

223 (LC-10AT, Shimadzu, Japan) analysis to quantify ~~the~~ eugenol

224 ~~concentrations.~~concentration. The HPLC was equipped with ~~the~~an InertSustain AQ-

225 C18 reverse phase column (4.6×250 mm, 5.0 μm, Shimadzu) and a UV-vis detector.

226 The mobile phase was a mixture of acetonitrile/H_2O (v/v: 60/40) at a flow rate of 0.6

227 mL/min, and the detection wavelength was ~~set at~~ 280 nm. The first-order kinetic rate

228 constant of eugenol degradation can be obtained from the slope of plot of $-\ln(c_t/c_0)$

229 versus reaction time as presented in Eq.(1).

230 $$\ln(c_t/c_0)=-kt \tag{1}$$

231 ~~Here,~~ Where c_0 ~~(μM)~~ and c_t ~~(μM)~~ are eugenol ~~concentration~~ concentrations

232 (in μM) at the initial and reaction time t~~:~~, while k ~~stands for~~represents the pseudo

233 first-order rate constant.

234 **2.3.2 UV-vis and fluorescent spectra**

235 The UV-vis light absorbance spectra of reacted solutions (placed in a 1 cm path

236 length quartz cuvette) were measured by using an UV-vis spectrophotometer (Specord

237 210 plus, Analytik ~~Jenal~~Jena,, Germany). The instrument ~~is~~has a dual-beam optical

238 system with tungsten and deuterium lamps as light sources. A reference absorption

239 spectrum of ultrapure water was carried out in the same cuvette prior to sample analysis

240 for baseline correction.

241 Immediately ~~following~~after the UV-Vis measurement, the cuvette was transferred

242 to a three-dimensional EEM fluorescence spectrometer (FluoroMax Plus，HORIBA

243 Scientific~~) to record variation of fluorescence intensity upon irradiation. Spectral~~). The

244 ranges of wavelength varied from 200 to 450 nm for excitation wavelengths (Ex) and

245 from 290~~-~~ to 650 nm for emission wavelength (Em). ~~Excitation~~Intervals of the

246 excitation and emission ~~wavelength intervals~~wavelengths were 5 nm and 2 nm ~~steps~~,

247 respectively. The reported absorbance and EEM spectra here are ~~the average~~averages

248 of the results from ~~triplicate~~ experiments in triplicate.

2.3.3 Determination of HULIS ~~concentration~~concentrations

250 Solid phase extraction (SPE) cartridges (CNW Poly-Sery HLB, 60mg/cartridge)

251 were used to isolate HULIS from the reaction ~~solution~~products. The ~~original~~ SPE

252 ~~cartridges~~cartridge was first rinsed with 1 mL ultrapure water and 3 mL methanol prior

253 to extraction. The solution was acidified to pH ~2 using HCl and loaded on an SPE

254 cartridge, ~~subsequently~~which was rinsed with 1 mL ultrapure water again. Next, 3 mL

255 methanol~~-~~/ammonia (98:2, v/v) mixture was added into the SPE cartridge to elute

256 HULIS~~ component~~, and the solution was ~~evaporated~~blew to full dryness with high~~-pure~~

257 purity N_2, followed by dilution with ultrapure water to 25 mL for quantification of

258 HULIS ~~with~~using the HPLC coupled with an evaporative light scattering detector

259 (ELSD3000). ~~The recovery~~Recovery efficiency of the HULIS standard~~-~~, Suwanne

260 River Fulvic Acid (SRFA), was 75-80% ~~and~~with the standard deviation of

261 reproducibility ~~test~~ less than 5%. More details have been described elsewhere (Tao et

262 al., 2021).

2.3.4 Oxidative ~~potential~~potentials (OPs) based on DTT assay

264 ~~We detected OP based on previous~~The OPs of reaction products were determined

265 by the DTT method (Cho et al., 2005; Lin and Yu, 2019) with ~~minor~~slight improvements.

266 Briefly, ~~a~~1.2 mL ~~portion of~~ sample solution was transferred into a 10 mL glass tube,

267 then 6 mL phosphate buffer (0.1 M, pH 7.4) and 300 µL of 2.5 mM DTT were added

268 and mixed thoroughly. The ~~samples were~~DTT mixed solution was placed in a 37℃

water bath for incubation some time, and reaction was terminated at 30 min intervals over. Over the course of reactions that lasted for 150 min by takingminutes, 1 mL aliquotsaliquot of DTT mixture was taken every 30 minutes, and adding 100 µL of 5 mM DTNB (prepared in 0.1 mM phosphate buffer) towas added and loaded in a centrifuge tube. Next, reactionreactions between DTNB and DTT produced bright yellow TNB, which was quantified usingby the UV-Vis spectrometer within 30 minminutes. Finally, we recordedmeasured the light absorbance (A_t) at 412 nm at time t to quantify indirectly quantify remaining DTT. Another 1.2 mL ultrapure water instead of sample solution was treated in the same way and the absorbance was denoted as A for distinguish from A_t. as blank value. A_0 represents the initial light absorbance value. Thus, theDTT concentration of DTTconsumed by the sample solution (M_{DTT}, µM) and that by the blank solution (M_{DTT0}, µM) werecan be calculated asaccording to Eq.(2) and Eq.(3), respectively.

$$M_{DTT} = \frac{A_0 - A_t}{A_0} \times C_{DTT\,0} \tag{2}$$

$$M_{DTT0} = \frac{A_0 - A}{A_0} \times C_{DTT\,0} \tag{3}$$

Here, C_{DTT0} was the initial DTT concentration in sample solution (100 µM in this work). DTT consumption raterates (R_{DTT} and R_{DTT0}) waswere then obtained from the slopeslopes of plotplots of M_{DTT} and M_{DTT0} versus incubation timetimes. Experiments of blanks and samples were typically run in a triplicate. The reproducibility of the whole analysis showed that the relative standard deviation of the DTT consumption rate analysis was 3-4%.

2.3.5 ProductProducts analysis by GC-MS

Reacted solution (about 30 mL) was extracted with 10 mL dichloromethane twice. The extracts wereextract was concentrated tointo 1 mL using gentleby blowing N_2 blow

12

293 ~~drying~~gently, subsequently transferred to a 2 mL vial, and analyzed ~~with~~by a GC-MS

294 (7890A GC/5975C MS, Agilent~~), using~~) with a DB-5ms capillary column (30 m×0.25

295 mm×0.5 μm). The operational conditions were set as follows: injector was at 200℃;

296 ion source was at 230 ℃; ~~The~~ column oven temperature was programmed~~:~~ to be held

297 at 35℃ for 4 ~~min~~minutes, then ramped to 250 ℃ at a rate of 20℃/~~min~~minute and held

298 for 10 ~~min~~minutes. The recovery efficiency, method detection limits and quality

299 assurance/quality control ~~has~~have been described in ~~detail elsewhere~~our previous work

300 (Ye et al., 2020).

2.3.6 SP-AMS analysis and ~~aqSOA~~ mass ~~yield~~yields <mark>of reaction products</mark>

302 An Aerodyne SP-AMS (Onasch et al., 2012) was applied to analyze the low

303 ~~volatile organics in reaction solution~~-volatility organic products, similar to our previous

304 work (Chen et al., 2020~~).~~; Ge et al., 2017). SP-AMS data were acquired in V mode and

305 analyzed by Squirrel v.1.56D and Pika v1.15D software. ~~All the~~The organic ~~fragment~~

306 ~~ions~~fragments were classified into six groups: CH, CHO, CHN, CHO_2, CHON~~,~~ and HO.

307 Elemental ratios (oxygen-to-carbon, O/C; hydrogen-to-carbon, H/C), were

308 ~~obtained~~calculated according to the method proposed by Canagaratna et al. (2015).

309 Since the AMS analysis requires ~~the~~ nebulization of sample solution into particles

310 before determination, and quantification of organics ~~in each experimental run depend~~

311 ~~on~~was influenced by the atomization efficiency and carrier gas flow, etc., we thus

312 cannot use SP-AMS ~~recorded~~measured concentration to quantify ~~aqSOA~~the mass of

313 products directly. In this case, according to ~~the method suggested by~~ Li et al. (2014),

314 we added an internal standard (SO_4^{2-}) prior to AMS analysis~~. The~~, and the mass ratio of

315 particle-phase organics to SO_4^{2-} ($\Delta Org/SO_4^{2-}$) ~~after atomization represented~~can be used

316 to calculate the ~~relative aqSOA~~ mass concentration of products. Furthermore,

13

317 ~~aqSOA~~the mass yield ~~(Y_SOA~~of aqueous-oxidation products ($Y_{products}$, %), which is the

318 mass of products generated ~~aqSOA mass~~per unit mass of precursor consumed, can be

319 calculated as Eq. (4).

$$\text{\sout{Y_{SOA}}}Y_{products}(\%)=\frac{(\Delta Org/SO_4^{2-})[SO_4^{2-}]_0}{c_0 M \eta} \times 100\% \tag{4}$$

321 Where $[SO_4^{2-}]_0$ is the ~~initially added~~ SO_4^{2-} concentration (here 7.27 mg·L^{-1}~~);~~), C_0 is the

322 initial eugenol concentration~~,~~ (in mmol/L~~;~~), M is ~~molecular weight~~MW of the precursor

323 (164 g/mol for eugenol) , and η is the ~~degradation efficiency~~degraded fraction of

324 eugenol.

3 Results and discussion

3.1 Kinetics of ~~the photo-oxidation~~aqueous photooxidation

327   Figure 1 shows unreacted eugenol concentrations (c_t) and the negative logarithm

328 of c_t/c_0 (-$\ln(c_t/c_0)$) as a function of reaction time, respectively. The pseudo first-order

329 rate ~~constant~~constants (k) obtained by Eq.(1) ~~was~~were also presented. ~~Error bars~~

330 ~~represent one standard deviation from triplicated measurements.~~ As described in

331 ~~Figure~~Fig. 1a, eugenol concentration decreased to be ~~lower than~~ ≤20% of the initial

332 concentration ~~at~~in 3 ~~h~~hours, suggesting photolysis was fast under ~~reaction~~all three

333 conditions. In the presence of $^3C^*$, eugenol was degraded ~~to~~nearly 100% after 3 ~~h~~hours.

334 Previous study (Chen et al., 2020) on $^3C^*$-initiated 4-ethylguaiacol ~~$^3C^*$-initiated~~

335 oxidation ~~(Chen et al., 2020) showed that it degraded completely until~~reports a time of

336 21 ~~h.~~hours for a complete degradation. Apart from difference of ~~target~~

337 ~~precursor~~precursors, different light irradiation spectra and stronger energy of light

338 ~~sources~~in this work than the previous work might be responsible for the fast loss of

339 eugenol. The <mark>bond dissociation energies (BDEs)</mark> are 340 kJ/mol for OH, 374 kJ/mol for

340   C-H in -CH$_3$ group, 345 kJ/mol for C-~~=~~C ~~in C=C bonds~~bond, and 403 kJ/mol for C-H

341   in -OCH$_3$ group, respectively (Herrmann et al., 2003; He et al., 2019). The lowest BDE

342   was found for the O-H bond and C-~~=~~C bond. Due to ~~the influence~~influences of steric

343   hindrance and intramolecular hydrogen bonding, the H-abstraction ~~reaction~~ from ~~the~~

344   OH group might ~~have been less~~not be favorable~~. The~~ and the most ~~favorable~~probable

345   H-abstraction ~~reaction~~ might ~~have taken~~take place in ~~the~~C-~~=~~C ~~in~~of the allyl group. As

346   a result~~of~~, breakage of C=C into C-C at the allyl group ~~site,~~ can lead to the formation

347   of 2-methoxy-4-propyl-phenol~~, could form (see~~ (Section 3.6.1). ~~As we known,~~

348   ~~when~~When photon energy is higher than ~~bond dissociation energy, they can directly~~

349   ~~break~~the BDE, chemical ~~bond of molecules~~bonds can break, leading to decomposition

350   of compounds and possibly further mineralization. The energies of photons at 300 and

351   350 nm ~~in our light sources~~ are 412 kJ/mol, and 353 kJ/mol, ~~which are~~higher than the

352   weakest ~~BDEs~~BDE in eugenol, ~~as a result, eugenol molecule~~therefore it can ~~directly~~

353   ~~absorb photo energy to decompose~~be easily decomposed after absorbing the photon.

354   As shown in Fig. 1b, the first-order rate constants were 2.43×10^{-4} s^{-1}, 2.73×10^{-4} s^{-}

355   ^{1}, and 5.75×10^{-4} s^{-1} for direct photolysis and ~~photooxidation~~photooxidations by •OH

356   and ^{3}C*, respectively. ^{3}C*-initiated ~~photodegradation~~photooxidation was quicker than

357   that ~~with •~~attacked by OH, likely due to combined contributions ~~of combination of~~

358   ~~multiple pathways including~~from reactions with ^{1}O$_2$, O$_2^{-•-}$ and ~~•~~OH~~. A similar~~ (Section

359   3.2). Similar results were found for aqueous phase ~~reaction~~reactions of three phenols

360   ~~with •~~against OH and ^{3}C* by Yu et al. (2016) ~~who showed degradation rates of three~~

361   ~~compounds~~(Note the initial concentrations of H$_2$O$_2$ and DMB were ~~all higher with ^{3}C*~~

362   ~~than •OH.~~100 µM and 5 µM, respectively, with the same ratio as 300 µM H$_2$O$_2$ to 15
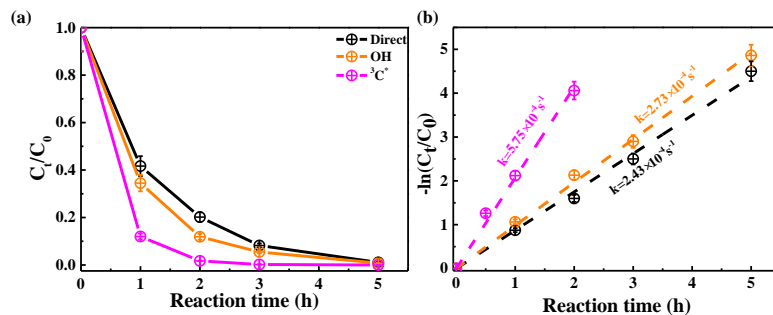
363   µM DMB in this work)

364

Figure 1. Aqueous- -phase eugenol decay kinetic curves (a) and ~~regressed first-order~~ rate constants (b) under three conditions. Error ~~bars represent~~bar represents one standard deviation from ~~replicated~~the measurements in triplicate.

3.2 Relative importance of ROS ~~to~~in photooxidation

3.2.~~1Quenching~~1 Quenching experiments in $^3C^*$-initiated photooxidation

Relative importance of <u>different</u> ROS in ~~photodegradation processes was usually~~ <mark>photooxidation</mark> can be investigated by ~~the~~ addition of radical <u>scavengers/</u>quenchers, and ~~here it was calculated~~ then be evaluated based on the different degradation efficiencies of eugenol in absence and presence of ~~different~~the corresponding ROS quenchers. For each ~~scavenger~~quencher, we conducted several gradient experiments with varying molar ratios of eugenol to ~~quenchers~~quencher. The ratios were ~~set as~~ 0.075:1, 0.15:1, 0.3:1, 0.75:1, 1.5:1 for quenchers of NaN_3, TMP and TBA, and 1.2:1, 1.6:1, 2.5:1, 5:1, 10:1 for SOD, which were all within the typical ~~range~~ranges of ~~molar ratios to quench~~ ROS <u>quenching experiments</u> reported previously (Zhou et al., 2018). ~~Above~~<mark>Excess</mark> concentrations of ~~the added quencher~~ quenchers have been <u>added</u> repeatedly ~~adjusted~~ to ensure the complete reactions between radicals and scavengers. Figure 2 displays the ~~effects~~impacts of ~~different ratios~~ quenchers on eugenol degradation. ~~As shown, when~~

~~adding quenchers into solution, all~~All rate constants (k) with quenchers were lower than those of the quencher-free solutions. The optimum molar ~~ratios~~ratio of eugenol to ~~quenchers were selected~~quencher was chosen when the inhibition degree of eugenol degradation unchanged with the increase of added quencher ~~mass ~~(Wang et al., 2021). For example, ~~upon decreasing ~~along with the decrease of molar ratios of eugenol to NaN$_3$ from 1.5:1 to 0.075:1, the inhibitory degree of eugenol degradation was ~~unchanged~~stabilized at the ratio of 0.15:1, indicating that ^{1}O$_2$ has been ~~absolutely~~completely quenched at this ratio, therefore a molar ratio of 0.15:1~~, so, we finally selected molar ratios of 0.15:1~~ for NaN$_3$ was optimal, since excess scavenger may ~~produce~~generate other products that ~~can change~~interfere the existing ~~reaction. Finally~~reactions. Similarly, the optimal molar ratios of eugenol to ~~quencher~~quenchers of TBA, NaN$_3$, TMP and SOD, ~~of ~~were determined to be 1.5, 0.15, 0.075 and 2.5 ~~were selected~~, respectively. ~~Table1~~Table 1 and ~~Figure~~Fig. S1 compared the rate constants determined under ~~various radical quenchers ~~the ratios above and ~~results showed that the ranking of first-order rate constants were ~~they were in an order of TMP<NaN$_3$<SOD<TBA, suggesting relative importance of generated ROS to eugenol degradation was in the order of ^{3}C*＞^{1}O$_2$＞O$_2$$^{\cdot-}$＞·OH. This result suggests that ^{3}C* plays a major role in the photooxidation ~~reaction. Other studies (~~. Previously, Laurentiis et al.~~.,~~. (2013~~;~~) reported that 4-carboxybenzophenone (70 μM) could act as ^{3}C* and the photosensitized degradation was more effective than oxidants such as OH, O$_3$, etc.; Misovich et al.~~.,~~. (2021) ~~of~~investigated the aqueous DMB-photosensitized reaction ~~also showed~~(5 μM, same as it in this study) also demonstrated that ^{3}C* was the greatest contributor to phenol or guaiacyl acetone ~~loss~~degradation, followed by ^{1}O$_2$, while both ·OH and ^{1}O$_2$ contributions were relatively minor.

~~The value of (~~We propose to use the following Eq.(5) to roughly assess the

17

contribution of a certain ROS (Ct_{ROS}) to eugenol degradation:

$$Ct_{ROS}=k_{ROS}/k = (k - k_{quencher})/k \quad (5)$$

Here k_{ROS} is the rate constant contributed by the ROS, which is defined as the difference between the original rate constant in $^3C^*$-initiated oxidation (k) and the rate constant after the target ROS has been completely scavenged by its corresponding quencher ($k_{quencher}$). k and $k_{quencher}$ in fact refer to those reported in Fig. S1b.

According to Eq.(5), Ct_{3C^*} was calculated to be 0.857, therefore contribution of $^3C^*$ was estimated to be as high as 85.7%. Similarly, the contributions of $^1O_2$, $O_2^{\bullet-}$ and $\bullet OH$ were 80.5%, 61.4% and 53.9%, respectively. The total contribution of the four ROS largely exceeded 100%. This can be explained by the fact that ROS scavengers can actually significantly interrupt the radical chain reactions as compared to those in the absence of scavengers. For instance, addition of TMP not only scavenges $^3C^*$, but also inhibits generation of $^1O_2$, $O_2^{\bullet-}$, etc. These findings suggest that we cannot directly precisely quantify the contribution of a ROS just on the basis of its scavenging efficiency, therefore the contributions calculated from Eq.(5) can only be used to compare the relative importance of different ROS. One should be cautious to apply quenching approach to quantify the role of ROS in complex reaction system. Determination of ROS concentrations during oxidation should be instead be an effective way to elucidate the role of ROS. Therefore, we tried to detect in-situ generated $\bullet OH$, $O_2^{\bullet-}$ and $^1O_2$ during photochemical reactions using a micro electron spin resonance (ESR) spectrometer (Bruker Magnettech, Berlin, Germany) with DMPO as the spin trap to form stable DMPO-$\bullet OH$ or DMPO-$O_2^{\bullet-}$, with TEMP to capture $^1O_2$ to produce TEMP-$^1O_2$ spin-adduct (TEMPO). The

18

amounts of radicals can be identified and quantified by the peak patterns in ESR spectra, such as the quarter line with a height ratio of 1:2:2:1 for DMPO-·OH, 1:1:1:1 for DMPO-$O_2^{\cdot-}$ and 1:1:1 for TEMP-$^1O_2$ (Guo et al., 2021). Unfortunately, OH radical cannot be detected since theits concentrations may not meetmight be lower than the detection limit of the instrument (Fig. S2, ESR spectra of ·OH). In contrast, we were able to detect higher concentrations of $^3C^*$ and found intensity of TEMP-$^1O_2$ signal reached its maximum at 30 minminutes, then decreased slowly (Fig. S2, ESR spectra of $^1O_2$). Combining the greatest inhibitive effect of TMP with high $^1O_2$ concentration from ESR method, we can conclude that $^3C^*$ and $^1O_2$ play relatively important roles in eugenol photodegradationphotooxidation.

Figure 2. Ratio of residue unreacted eugenol concentration to its initial concentration (C_t/C_0) at different molemolar ratios of eugenol to quencher, as a function of reaction time with: (a) TBA quencher, (b) NaN₃ quencher, (c) TMP quencher and (d) SOD quencher. Legend represented mole ratios of eugenol to quenchers.

3.2.2 Quenching experiments in OH-initiated photooxidation

To examine the contributions of ~~the quenchers~~ROS to eugenol degradation for OH-initiated oxidation, TBA and p-BQ as trapping ~~agent~~agents were added. Similar to $^3C^*$-initiated oxidation, several gradient experiments ~~via~~with varying molar ratios of eugenol to quenchers were conducted. The ratios were set as 6.5:1, 3.2:1, 1.6:1, 1.1:1 and 0.8:1 for p-BQ and 3.0:1, 1.5:1, 0.75:1, 0.3:1 and 0.15:1 for TBA. According to Fig. S3, molar ratio only had a slight influence on eugenol degradation, although degradation can be inhibited effectively by quenchers. ~~So~~Thus, we ~~finally selected appropriated~~determined the appropriate molar ratios of ~~eugenol to quenchers:~~ 0.8 and 0.75 for p-BQ and TBA, respectively, ~~since adding too high concentrations of~~as excess scavengers ~~can actually~~might influence the chemical ~~reaction~~reactions.

Variations ~~in~~of the rate constants for ~~above~~the aforementioned quenching experiments were ~~calculated, respectively~~determined, in comparison with ~~tests~~those conducted without quenchers, and the results ~~were~~are listed in Table 1 and presented in Fig. S4. For TBA quenching tests, the rate constant decreased by 18.7% (from 2.73×10^{-4} s^{-1} to 2.22×10^{-4} s^{-1}), showing that $\cdot$OH radical played a certain role in eugenol photooxidation. Since H_2O_2 was mainly photolyzed at wavelength <300 nm to generate OH radical, ~~but~~ irradiation above 300 nm ~~here~~ did not ~~dominate.~~affect the reaction significantly. The p-BQ could quench $O_2^{\cdot-}$, ~~which~~ further ~~suppress~~suppressing the generation of other ROS (e.g., $\cdot HO_2$), ~~as a result,~~therefore the rate constant decreased the most (from 2.73×10^{-4} s^{-1} to 1.20×10^{-4} s^{-1}), suggesting $O_2^{\cdot-}$ ~~might be responsible~~was important for eugenol ~~photodegradation~~photooxidation. This hypothesis could be further confirmed by the decline of rate constant under N_2-saturated solution ~~shown later.~~(Section 3.2.3). However, it was difficult to detect both $\cdot$OH and $O_2^{\cdot-}$ directly due to their relatively short ~~half-life~~lifetimes and low ~~concentration~~concentrations via ESR

20

473   in this work.

474

Table 1. The ~~reaction~~first-order rate constants of eugenol in the presence of various scavengers. The ~~experiment~~initial conditions were as follows: ~~0.3 mM~~300 μM eugenol~~,~~; molar ratios of eugenol to ~~quencher~~quenchers TBA, NaN$_3$, TMP and SOD, of 1.5, 0.15, 0.075 and 2.5, respectively; ~~mole ratio~~molar ratios of eugenol to ~~quencher~~quenchers p-BQ and TBA of 0.8 and 0.75, respectively.
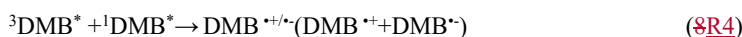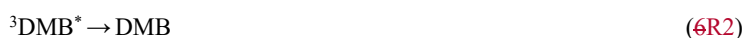
^{3}C*-initiated quenching experiments			
~~quenchers~~Quenchers	ROS	~~reaction~~Reaction rate constant k (s^{-1})	Pearson's R^2
no quencher	-	5.75×10^{-4}	0.996
TBA	•OH	2.65×10^{-4}	0.999
SOD	O$_2$·$^-$	2.22×10^{-4}	0.995
NaN$_3$	^{1}O$_2$	1.12×10^{-4}	0.999
TMP	^{3}C*	0.82×10^{-4}	0.999
•OH-initiated quenching experiments			
~~quenchers~~Quenchers	ROS	~~reaction~~Reaction rate constant k (s^{-1})	R^2
No quencher	-	2.73×10^{-4}	0.995
TBA	•OH	2.22×10^{-4}	0.998
p-BQ	O$_2$·$^-$	1.20×10^{-4}	0.995

3.2.3 Influences of different saturated gases

In order to assess the role of O$_2$ in ~~the mechanism of~~ eugenol photolysis, a ~~few~~series of experiments were performed under both O$_2$-saturated and N$_2$-saturated ~~instead of~~ conditions in addition to air. N$_2$ gas was purged into reaction solution for ~30 ~~min~~minutes before experiment to achieve ~~deoxygenated~~the O$_2$-free condition. Figure 3 compared the changes of eugenol ~~loss variations~~concentrations and rate constants (see insets) under three ~~saturated~~gas conditions for direct photolysis, OH-initiated and ^{3}C*-initiated ~~oxidation~~oxidations, respectively. The ~~insets of the Fig.3a, 3b and 3c showed the corresponding~~ rate constants. ~~The rate constants under O$_2$, air and N$_2$~~ followed the order of k$_{O_2}$ > k$_{Air}$ > k$_{N_2}$ under both direct photolysis and •OH oxidation, providing evidence in support of O$_2$ being ~~responsible~~significant for eugenol degradation. This
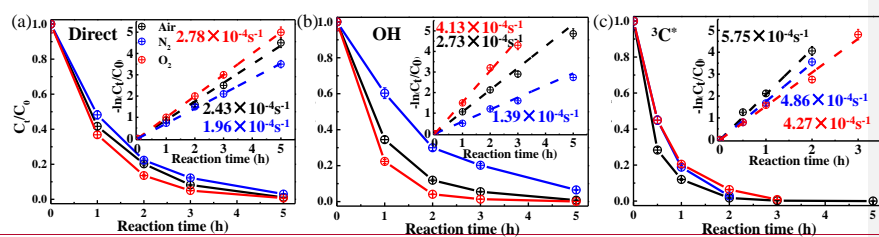
491 might be explained by the fact that O_2 can act as an electron acceptor to generate $O_2^{•-}$

492 and $•HO_2•$, and subsequently form H_2O_2 and $•OH$. For direct photolysis, rate constant

493 under O_2-saturated condition increased 14.4% while it decreased 19.3% under N_2

494 saturation, ~~in contrast to the case of~~ <u>from that under</u> saturated air. For OH-initiated

495 oxidation, the difference of rate constants under three saturated gases became more

496 distinct.

497 On the contrary, rate constants followed the order of $k_{Air} > k_{N_2} > k_{O_2}$ in $^3C^*$-

498 initiated oxidation ~~system~~. There are two possible explanations. On ~~the~~ one hand,

499 ~~in~~<u>under</u> N_2-saturated ~~solutions~~<u>condition without oxygen</u>, DMB would ~~be~~

500 ~~involved~~<u>involve</u> in reactions (~~5-8), followed by~~<u>R1-R4), leading to a</u> more effective

501 generation of $^3DMB^*$~~. For this reason, eugenol~~ <u>* therefore a higher</u> degradation

502 efficiency ~~was higher under N_2 atmosphere~~ than ~~in~~<u>under</u> O_2-saturated ~~solution~~<u>condition</u>.

503 On the other hand, ~~in~~<u>for</u> air/O_2-saturated solutions, irradiation of DMB and eugenol

504 would involve <u>also</u> reactions (~~5-12),~~<u>R5-R8) in addition to (R1-R4), and</u> as a result, the

505 amount of $^3DMB^*$ radical decreased, ~~accompanied by the~~<u>due to</u> formation of other ROS

506 ($^1O_2$, $O_2^{•-}$, $•OH$, etc) with relatively weak oxidative ~~capacity~~<u>capacities</u>. In summary,

507 quenching of $^3DMB^*$ by ground state molecular oxygen could account for the ~~lower~~<u>low</u>

508 degradation efficiency in O_2-saturated condition.

509 $$DMB + hv \rightarrow {}^1DMB^* \rightarrow {}^3DMB^* \qquad\qquad (\text{~~5~~R1})$$

510 $$^3DMB^* \rightarrow DMB \qquad\qquad (\text{~~6~~R2})$$

511 $$^3DMB^* \rightarrow Products \qquad\qquad (\text{~~7~~R3})$$

512 $$^3DMB^* + {}^1DMB^* \rightarrow DMB^{•+/•-}(DMB^{•+} + DMB^{•-}) \qquad\qquad (\text{~~8~~R4})$$

513 $$^3DMB^* + O_2 \rightarrow DMB + {}^1O_2 \qquad\qquad (\text{~~9~~R5})$$

514 $$DMB^{•-} + O_2 \rightarrow •DOM^+ + O_2^{•-} \qquad\qquad (\text{~~10~~R6})$$

515 $$O_2^{•-} + 2H^+ \rightarrow H_2O_2 + O_2 \qquad\qquad (\text{~~11~~R7})$$

23

516      $H_2O_2 \rightarrow$ ~~2·OH~~   (~~122~~$2OH$

517   (R8)
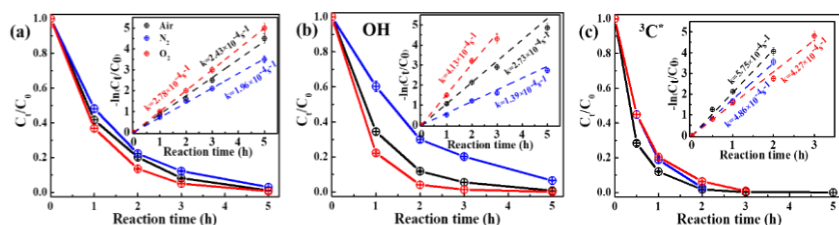
518

519

520

521

Figure 3. Ratio of ~~remaining~~unreacted eugenol concentration to its initial concentration (C_t/C_0) as a function of reaction time at different saturated gases under (a) direct photolysis (b) OH-initiated oxidation and (c) $^3C^*$-initiated oxidation. ~~Insert plots represented eugenol consumption versus reaction time under different saturated gases:~~The insets in (a ~~direct photolysis (b) OH initiated and (~~c) ~~$^3C^*$-initiated photooxidation.~~show the corresponding rate constants.

3.2.4 ~~Variation~~Variations of pH ~~value~~and dissolved oxygen

The initial pH values ~~in~~of reaction solutions for direct photolysis and OH-initiated oxidation were unadjusted, while ~~initial pH~~those for the $^3C^*$ ~~system~~-oxidation was adjusted to 3. The variation of solution pH ~~were~~is presented in Fig. 4a. ~~As shown in Fig.4a, solution~~The pH values decreased ~~quickly~~dramatically at the beginning of illumination (from 7.4 to ~5.0 ~~for~~in the first ~~1h~~1 hour) then tended to ~~smooth in~~be flat for both direct photolysis and OH-initiated oxidation. However, little change of pH ~~value~~(less than 0.1 unit) was observed for the $^3C^*$-initiated photooxidation~~, which could be ascribed~~ throughout the oxidation, likely ascribing to ~~very~~its low initial pH ~~value (~~of 3. Note a small amount of acids can change solution pH significantly when original pH~~=3)~~ is high, but ~~Generally speaking, slight increase of acidity~~ cannot change pH remarkably ~~change pH value~~when the original solution pH was ~~very~~low. ~~We~~Therefore, we cannot rule out formation of ~~acid~~acidic products ~~at~~(such as organic acids) during $^3C^*$-initiated oxidation. ~~Thus, the decrease of pH value might be related to formation of~~

organic acid and HULIS since carboxylic acids are possibly abundant in HULIS (Huo et al., 2021; Salma et al., 2008). as during direct photolysis and OH-initiated oxidation.

OxygenAs discussed in Section 3.2.3, oxygen can take part in photochemical reaction to form ROS, which may in turn destroy the structure of precursors. In order to further confirm the role of O_2,precursor. Here we measured the oxygen consumption via determining concentrationduring oxidation through determination of dissolved oxygen (DO) contents by a dissolved oxygen meter (Seven2Go Pro S9, Zurich, Switzerland) during the photochemical process.). DO was consumed mainly at the first 1 hhour and keptremained stable afterwards with the increase of reaction time further increasing (Fig.(Figs. 4b-c and Fig. S5). PercentageThe amounts of consumed DO concentration consumption followed in the order of $^3C^*$>·>OH>direct photolysis. The maximum consumed DO consumption for was found in $^3C^*$-initiated oxidation process, which can be explained by the transfer of electrons from $^3C^*$ to O_2 to form $^1O_2$, which was thea major contributor to eugenol degradation. Obviously, a steady-state DO level was reached when the consumption rate was equal to the diffusion of O_2 into the solution (Pan et al., 2020). Overall, these results re-emphasize that O_2 can influence eugenol degradation and radical transformation via induction of radical chain reactions.

In summary, above experimental results confirmed that O_2 influenced eugenol decomposition and radical conversion via inducing radical chain reactions.
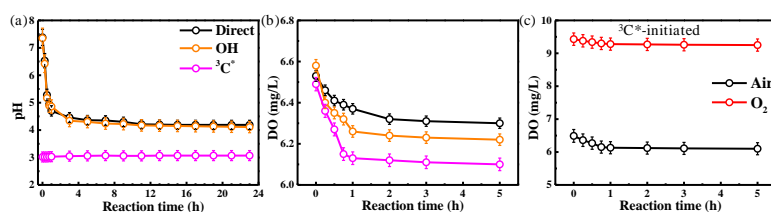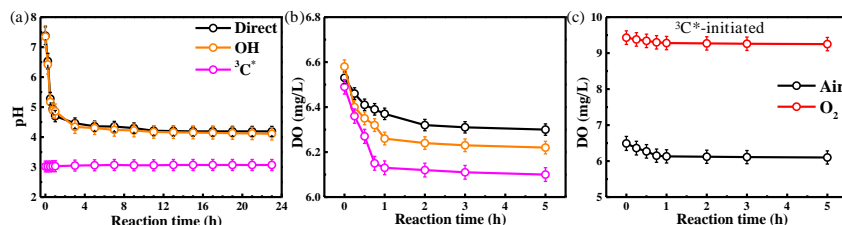
Figure 4. (a) pH values and (b) ~~(c)~~ dissolve oxygen ~~as a function of~~(DO) contents against reaction time under three photolysis conditions, and (c) DO contents during $^3C^*$-initiated oxidation under air or O_2-saturated conditions.

3.3 Optical properties of reaction products

3.3.1 Light-absorbing properties

The UV-vis light absorption spectra of the solutions at different reaction ~~time~~times are presented in Fig. 5. ~~According to UV-vis spectrum, the wavelength of significant~~ The light absorption by eugenol ~~ranges from 260 nm to~~itself mainly occurs in the range of 260-300 nm (n→π* electronic ~~transitions~~transition, 270-350 nm), which ~~in part in~~overlaps with the ~~field~~major photon fluxes (280 and 500 nm) of ~~photon fluxes in~~our lamp~~.~~ for photooxidations. Therefore, we can clearly observe that the characteristic absorption peak at 280 nm of precursor decreased ~~under~~ with the propagation of direct photolysis~~. As seen in~~ (Fig. ~~5, when adding oxidant H2O2, the total variation trend of absorbance was~~5a), similar to that ~~without oxidant.~~in OH-initiated photooxidation (Fig. 5b). However, the reaction was ~~extremely~~ quick in the presence of $^3C^*$, and the characteristic absorption peak at 280 nm after 3 ~~h irradiation~~ hours of illumination almost disappeared, suggesting nearly complete loss of eugenol, ~~which coincided~~consistent with the results in Section 3.1 that more than 99% eugenol was degraded ~~at~~in 3 ~~h~~hours. Additionally, there ~~is~~was an ~~increase in~~obvious absorption enhancement at longer wavelengths (300-400 nm) ~~over photoreaction, where~~during the

27

~~original~~photooxidation, whereas eugenol itself did not absorb ~~slight, suggesting~~light in this range, indicating some light-absorbing products (e.g., brown carbon~~) appeared.~~ (BrC) species) were generated. Aqueous ~~photodegradation~~photooxidation of some phenolic compounds (e.g., vanillic acid) also ~~observed~~presented long-wavelength (300-400nm) light absorbance, with intensity increasing with illumination time (Tang et al, 2020; Zhao et al., 2015~~), intensity of which also increased with illumination time.~~). In ~~comparison~~addition, there ~~are~~were some differences for light absorbance at wavelength of 300-400 nm in the three cases. For direct photolysis and OH-initiated oxidation, light absorbance increased during the first 15 ~~h~~hours, then remained at a plateau until 23 ~~h.~~ ~~however~~hours. However, for $^3C^*$-initiated oxidation, light absorbance increased during the first 7 ~~h~~hours, then decreased slowly afterwards. The different shapes of UV-vis spectra ~~of photooxidation by •~~between OH and $^3C^*$ ~~might be attributed to different~~ ~~reaction mechanisms, leading to the formation~~photooxidations indicate formations of different products.

 ~~The increase~~ Compared to the light spectrum of eugenol, there were also increases of light absorbance at ~~250~~~260 nm ($\pi\to\pi^*$ electronic transitions) upon aqueous ~~photo processing demonstrates~~photolysis in all three conditions (Fig. 5), demonstrating the generation of new substances likely with both~~the~~ aromatic C=C and carbonyl (C=O) functional groups (Tang et al., 2020). The enhancement at 300-400 nm ~~suggested the probability of HULIS formation because HULIS usually has~~may point to products with high ~~molecular weight~~MWs and conjugated structures~~.~~, possibly linking with HULIS or oligomers. Unfortunately, we ~~did not obtain~~were unable to quantify relative contributions of ~~reaction~~individual products to the overall light absorbance between 300 to 400 nm ~~because of~~due to lack of ~~specific component~~the full speciation of products and their light absorption spectra.
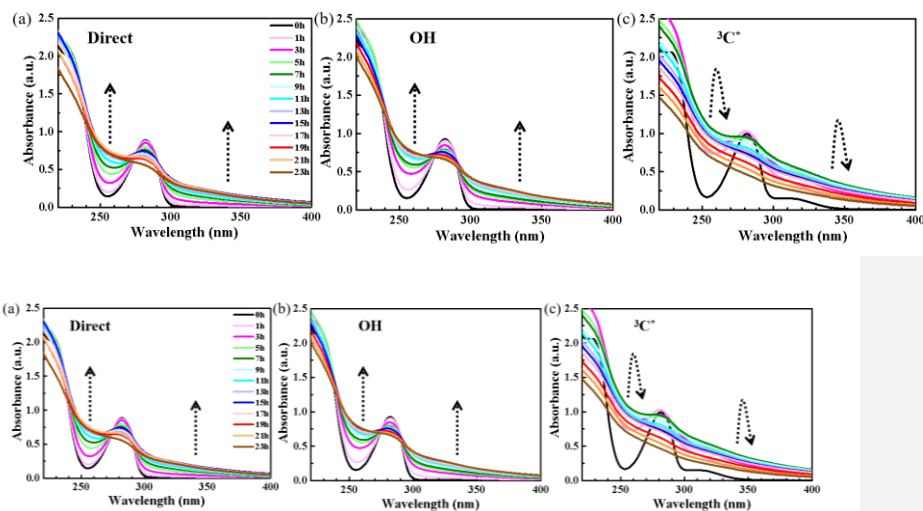
28

Figure 5. UV–vis light absorption spectra of reacted solutions at different reaction times under (a) direct photolysis, (b) OH-initiated oxidation, and (c)^{3}C*-initiated photooxidationoxidation.

3.3.2 Fluorescence properties

The variation of fluorescence intensitiesproperties of solutions before (0 hhour) and uponduring photolysis (3 h and 7 hhours) were investigated via the EEM technique, as shown in Fig. 6. For comparison, we also presented EEM profiles of pure eugenol (non-irradiated solution), pure DMB, and the end solutions (23 hhours) of direct photolysis and OH-initiated oxidation (in Fig. S6). The peaks at Excitation/Emission (Ex/Em=)=275/313 nm are ascribedcan be attributed to fluorescence of the phenolic structure of parent substance, (eugenol here), as suggested by Laurentiis et al. (2013). As shown in both Fig. 6 and Fig. S6, the fluorescence intensity from parent substance decreased after photolysis due to eugenol decay, and the decreasing trendreduction was very fast for ^{3}C*-initiated oxidation. This finding matchedmatches with the fast photolysis and large rate constant for ^{3}C*-initiated oxidation. The EEM plots for direct

29

photolysis and OH-initiated ~~reaction~~oxidation had similar contour patterns as shown in ~~Fig.6 a~~Figs. 6a and b ~~across the entire photochemical reaction~~, although EEM ~~profile~~profiles changed significantly with irradiation time. We also observed distinct fluorescent peaks at Ex/Em=235~~/~~/(400-500) nm, indicating that ~~irradiation caused~~illumination can cause a red shift in fluorescence emission wavelength. As suggested by Chang et al. (2010), fluorophores at Ex/Em=240/400 nm ~~was~~are linked ~~to~~with aromatic structures and condensed saturated bonds including polycyclic aromatic hydrocarbons. Another work (Li et al., 2021) showed that red shift in the fluorescence spectra was usually related to an increase in the size of ~~the~~ring system and an increase in the degree of conjugation. Previous studies (Chen et al., 2016a; Chen et al., 2019; Laurentiis et al., 2013; Wu et al., 2019) have reported that fluorescent compounds with emission wavelength at 400-500 nm may be highly oxygenated species such as HULIS. Additionally, HULIS have two typical fluorescent peaks in EEM ~~plots~~profile at Ex/Em=~~=~~(200-300~~/~~)/(400-~~500nm~~500) nm and Ex/Em=350~~/~~/(400-~~500nm~~500) nm with the former one having a higher intensity ~~for the former~~ (Graber and Rudich, 2006; Laurentiis et al., 2013; Vione et al., 2019; Wu et al., 2021). There was also evidence ~~(Bianco et al., 2014) to suggest~~ that direct photolysis of tyrosine and 4-phenoxyphenol generated HULIS with new fluorescence signals at Ex/Em=~~=~~(200~~-~~-250~~/~~)/(400~~-~~-450) nm and 300~~/~~/(400~~-~~-450) nm~~. So~~ (Bianco et al., 2014). In this regard, we inferred that new peak at Ex/Em=235~~/~~/(400-500) nm here ~~was~~ likely attributed to ~~chromophores of~~ HULIS. For the $^3C^*$-initiated ~~reaction~~photolysis, extra fluorescent peaks at Ex/Em=~~=~~(220-300~~nm/~~)/(400-~~500nm also~~500) nm appeared ~~at~~in the first 1 ~~h~~hour (data not shown), but their intensities ~~were much weaker~~weakened and gradually disappeared upon prolonged photolysis (3 ~~h). Anyway~~hours). Nevertheless, EEM results ~~were difficult to interpret~~should be interpreted with caveats because ~~of~~many

30

complicated substances ~~in reaction samples that~~ might contribute to absorption and
emission at <u>a</u> certain ~~excitation~~ wavelength, and it is hard to distinguish and isolate
fluorescent and nonfluorescent constituents ~~via current techniques. However, we can~~
~~inferred oligomerization reaction likely took place since oligomers emit fluorescence at~~
~~approximately 400 nm (Barsotti et al., 2016).~~<u>simply via the EEM</u> <mark>technique.</mark>

Another interesting finding was that a small fluorescence peak appeared at
Ex/Em$=$<u>$=$</u>(300-350<u>/</u>)/(300-350<u>)</u> nm ~~at different reaction stages.~~ <u>in some of the EEM</u>
<u>profiles.</u> Specifically, it appeared earlier for $^3C^*$<u>-*</u>-oxidation (at 3 ~~h~~<u>hours</u>) than <u>the</u> other
two systems, ~~and the peak~~<u>yet its intensity</u> seemed to be a bit stronger in the end
solutions of direct photolysis and OH-<u>-</u>oxidation (Fig. S6). EEM fluorescence spectra
~~for~~<u>of</u> HULIS from fog water <u>are reported to</u> have peaks at shorter excitation and
emission wavelengths than <u>those of</u> terrestrial fulvic acids<u>,</u> ~~suggesting a lower content~~
~~of aromatic structures and condensed unsaturated bond systems~~ (Graber and Rudich,
2006). Moreover, as suggested by Leenheer and Croue (2003), fluorescence peak
position of the ~~Ex/Em~~ maximum ~~of~~<u>Ex/Em for</u> HULIS with lower ~~molecular weight~~
~~shifted~~<u>MWs would shift</u> towards lower wavelengths, thus, we inferred fluorescence
peak at Ex/Em$=$<u>$=$</u>(300-350<u>/</u>)/(300-350<u>)</u> nm might be in part attributed to ~~small organic~~
~~acid. One unexpected phenomenon in the EEM spectra here is~~ the ~~absence of~~
~~fluorescence at higher excitation wavelengths (>350 nm), which is often observed in~~
~~aerosol particles (Wu et al., 2021). This could be attributed to different precursor and~~
~~aqueous reaction mechanisms (Xie et al. 2016).~~

~~Note that~~<mark>organic acids with only a few carbon atoms.</mark> Nevertheless, large
uncertainties still exist in using EEM fluorescence technique to ~~characterize~~<u>identify</u>
molecular ~~composition~~<u>compositions of the products</u> due to lack of standard EEM
~~profile~~<u>profiles</u> for specific ~~products of~~<u>compounds from</u> aqueous phase oxidation and
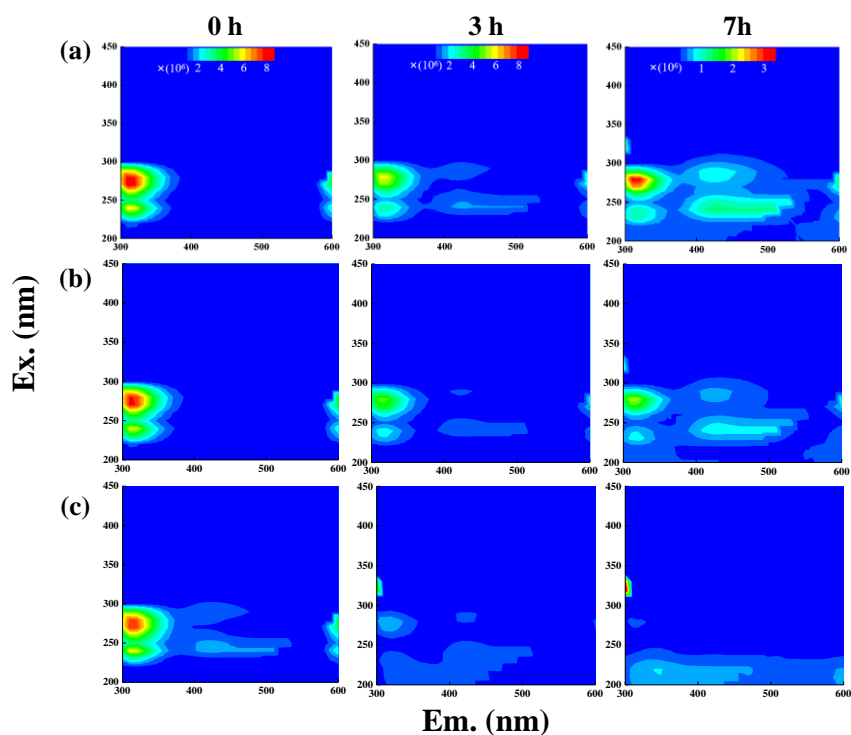
674 clearly more studies are needed in future.
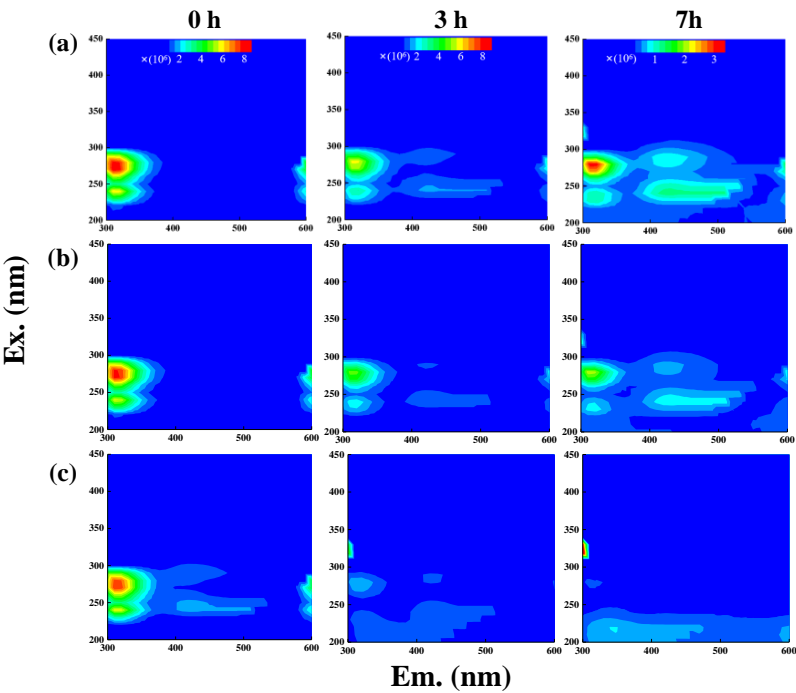
Figure 6. EEM fluorescence spectra of the initial solution (0 ~~h~~hour) and those at different reaction time (3 ~~h~~and 7 ~~h~~hours) under (a) direct photolysis, (b) OH-initiated _oxidation,_ and (c) $^3C^*$-initiated oxidation. ~~The top color bar represents the range~~

3.4 Characteristics of ~~fluorescence intensity.~~

3.4 **HULIS** ~~concentration determination~~

The EEM spectra ~~found~~revealed new prominent fluorescent peak at Ex/Em=250 ~~nm/~~(400-500) nm, which was likely ~~attributed~~owing to ~~chromophores of~~ HULIS. ~~Humic substances are subdivided~~HULIS can be divided into fulvic acid (water soluble at all pHs), humic acid (base soluble, acid ~~(pH 1)~~insoluble) and humin (insoluble at all pHs). In principle, extracted HULIS in this work with polymer-based HLB SPE packing ~~included~~include LMW organic acids, fulvic acids ~~or~~and other humic substances. ~~As suggested by Graber and Rudich (2006), two distinct ranges have been found to characterize humic substances: Ex/Em=330-350/420-480 nm (fulvic-like), and Ex/Em=250-260/380-480nm (humic-like). So, we inferred most HULIS in this paper was humic-like substance rather than fulvic-like substance. However, EEM technique cannot directly distinguish products solely based on the shapes and limited information of the EEM profiles. Here we determined the HULIS concentrations in the oxidized solutions by using the HPLC method.~~

Figure 7 ~~presented~~presents the measured HULIS concentrations ~~as a function of~~against the reaction time. The results show clearly that aqueous-phase eugenol oxidation ~~can produce~~is a source of HULIS, and the amount increased gradually in the first 7 ~~h~~hours, then remained at a similar level (about 30 mg/L) ~~later in~~for the OH-initiated oxidation. For direct photolysis, HULIS concentration increased until ~~11h~~11 hours and then ~~retained~~became steady at a level around 40 mg/L. For the $^3C^*$-oxidation, HULIS concentration increased to ~~its~~a maximum at 7 ~~h, but it decreased~~hours, then declined slightly afterwards. ~~The possible~~A plausible reason ~~was~~of such variabilities is that generated HULIS was capable of further taking part in photochemical reactions

705 since it can act as ~~photosensitizers. Study from Smith (2015) suggested different~~

706 ~~reaction mechanisms between aqueous benzene diols with~~ photosensitizer. Moreover,

707 Yu et al. (2016) characterized the products from aqueous oxidations of phenols by $^3C^*$

708 and OH ~~radical, with~~ radicals, and found both could produce oligomers and

709 hydroxylated species but the $^3C^*$ ~~oxidation producing highe molecular weight products~~

710 ~~with less fragmentation. Thus, we inferred that~~ *-oxidation could produce more ~~higher~~

711 ~~molecular weight HULIS were formed at the first stage due to oligomerization and~~

712 ~~functionalization as suggested by Jiang et al.(2021), which consequently~~of these

713 compounds when 50% of the precursor was reacted. Considering the large increases of

714 HULIS in the first 7 hours and the much faster increase of $^3C^*$-oxidation in the first 3

715 hours shown in Fig. 7, we postulate that HULIS species might overlap with the products

716 of high MW oligomers, which can in turn contributed to fluorescence at ~~Ex~~emission of

717 ~400 nm (Barsotti et al., 2016).

718 .

719
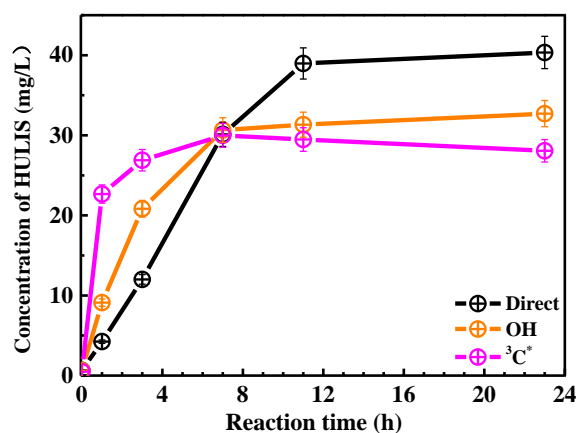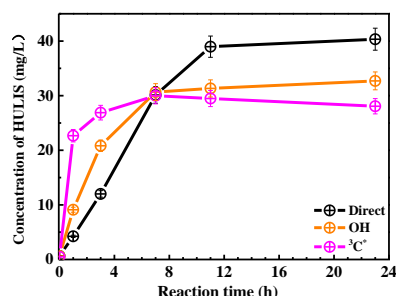
Figure 7. HULIS concentrations as a function of reaction time for the three ~~systems~~conditions

3.5 ~~aqSOA mass~~Mass yield and oxidation degree of reaction products

3.5.1 ~~aqSOA mass yield~~Mass yields

Figure 8a ~~showed~~shows SP-AMS measured organic mass profiles (normalized by sulfate mass, $\Delta Org/SO_4^{2-}$) against the reaction time. As the reaction propagated, $\Delta Org/SO_4^{2-}$ increased continuously in $^3C^*$-initiated system. Nevertheless it ~~rise gradually~~arose stepwise and reached a maximum at 19 ~~h~~hours, then remained at a plateau for the direct photolysis and OH-~~initiated~~mediated oxidation. Figure 8b ~~illustrated~~illustrates the calculated ~~aqSOA~~ mass yields at different reaction ~~time~~times. The ~~aqSOA~~ mass yields after ~~1h~~1 hour of illumination were in the ranges of 46.2%-196.5%, 22.1%-144.9%, 19.3%-140.1% for $^3C^*$-oxidation~~ by $^3C^*$~~, OH ~~radical~~ oxidation and direct photolysis, respectively. ~~The SOA mass yield are slightly higher than value (ranging from 80-140%) from phenol-triplet reaction (Ma et al., 2021; Smith et al., 2016; Yu et al., 2014).~~ For the same oxidation time, mass ~~yields~~yield from $^3C^*$-oxidation ~~were~~was generally higher than those from OH-~~initiated~~ oxidation and direct photolysis. ~~These results were similar to investigation on aqueous oxidation of phenolic compounds (Smith et al., 2014, 2015, 2016).~~ There are two plausible ~~reason for high~~

738 ~~masses~~reasons for high mass yield of $^3C^*$-initiated oxidation. ~~Firstly~~First, oxidation by

739 $^3C^*$ was more ~~efficiently~~efficient to form oligomers and functionalized/oxygenated

740 products (Richards-Henderson et al., 2014; Yu et al., 2016). Higher oxidative degree of

741 ~~aqSOA~~products from $^3C^*$-initiated photooxidation (see Sec.3.5.2) ~~warrants above~~

742 supports this hypothesis. Secondly, more light-absorbing products ~~(i.e. HULIS) can~~

743 ~~participate in SOA formation~~ formed during initial stage of $^3C^*$-oxidation (Fig. 5c) may

744 accelerate oxidation by acting as photosensitizers (Tsui et al., 2018).

745 　　The ~~aqSOA~~product mass yields obtained in ~~OH-initiated oxidation of~~this work

746 (~20%-197%) overall agree ~~well~~ with ~~that~~those reported previously for phenolic

747 ~~carbonyls, that is,~~compounds. For examples, Huang et al. (2018) reported mass yields

748 of 30-120% for syringaldehyde ~~(Huang et al., 2018).~~and acetosyringone; Smith et al.

749 (2014) found that mass yields of aqSOA from three phenols with $^3C^*$ were nearly 100%,

750 and Ma et al. (2021) reported a yield ranging from 59 to 99% for six highly substituted

751 phenols with $^3C^*$; Mass yields of SOA from three benzene-diols were near 100% with

752 both OH and $^3C^*$ oxidants (Smith et al., 2015); Direct photolysis of phenolic carbonyls,

753 and oxidation of syringol by $^3C^*$, had SOA mass yields ranging from 80 to 140% (Smith

754 et al., 2016). Our previous study on eugenol OH oxidation illuminated by a 500 W Xe

755 lamp reported ~~the aqSOA~~a mass yield of ~180% ~~for eugenol~~ (Ye et al., 2020), slightly

756 higher than the value ~~reported~~determined here owing to different simulated ~~solar~~
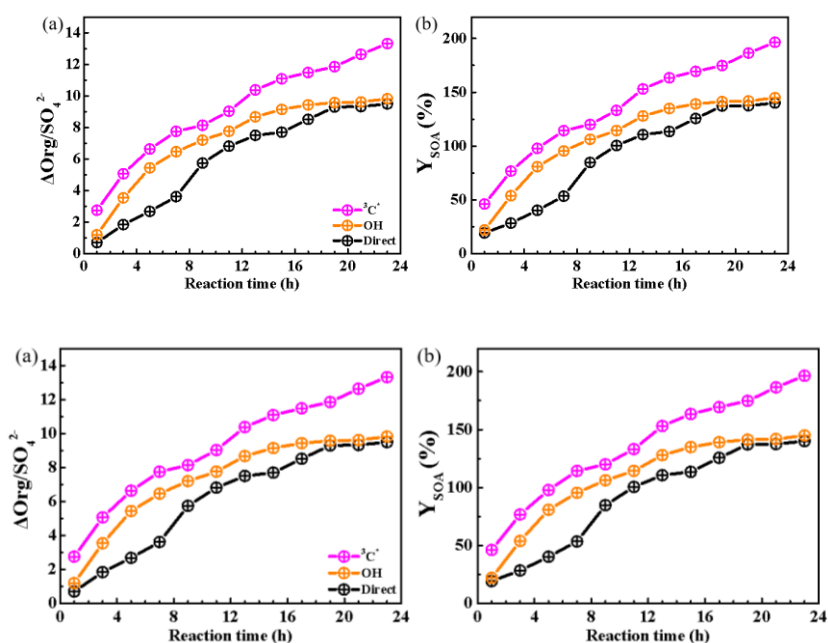
757 ~~irradiation~~lights.

Figure 8. Variations of the ~~aqSOA~~organic mass normalized by sulfate (a) (ΔOrg/SO_4^{2-}) and (b) ~~aqSOA~~ mass yields of reaction products with reaction time under three conditions.

3.5.2 Oxidation ~~degrees of aqSOA~~degree

In order to further ~~represent the~~probe oxidation levels of the ~~aqSOA~~reaction products, O/C derived from SP-AMS mass spectrum of the organics was used to ~~assess~~represent the oxidation degree of ~~aqSOA~~products. In addition, carbon oxidation state (OSc, defined as 2*O/C - H/C) was also calculated (Kroll et al., 2011). ~~Figure~~Figures 9a-c ~~described~~depict variations of the elemental ratios (O/C and H/C) and OSc ~~over time.~~during oxidations. Dramatic increases of O/C and OSc ~~in~~during the initial stage of oxidation (within 1 hour) were observed, with O/C ~~changed~~changing from 0.26 to 0.65, from 0.26 to 0.70, from 0.25 to 0.75, as well as OSc ~~changed~~ from -1.11 to -0.15, from -1.16 to -0.05, from -1.13 to 0.09 for direct photolysis ~~and~~, OH-

773 oxidation ~~by OH~~ and $^3C^*$~~,~~*-oxidation, respectively. The O/C was lower than ~~that~~those

774 of other phenolic aqSOA ~~reported~~ (Yu et al., 2014) due to different substituted

775 ~~group~~groups in aromatic ring ~~for~~of the precursors. Both O/C and OSc gradually

776 increased, while H/C ~~decreased for the first~~changed little after 1 ~~h then leveled off.~~hour.

777 The enhancements of OSc ~~at 23 h reached~~in the end were 1.22, 1.11 and 0.86 for $^3C^*$-

778 initiated oxidation, OH-initiated oxidation and direct photolysis, respectively.

779 Furthermore, the f_{44} vs. f_{43} ~~diagrams (termed as~~ diagram ("triangle plot") can be

780 used to demonstrate the evolution of ~~aqSOA~~SOA during oxidation (~~Fig. 9d f~~Ng et al.,

781 2010). The f_{44} and f_{43} are defined as the ratios of signal intensities of m/z 44~~(~~ (mainly

782 CO_2^+) and 43 (~~mostly~~mainly $C_2H_3O^+$) to the total organics. ~~As we known, CHO_2+ ion~~

783 ~~in the AMS spectra is an indicator for the carboxyl functional group (Jiang~~The~~ et al.,~~

784 ~~2021). Thus, our~~ results that the f_{44} ~~rise~~increased continuously (moved upwards)

785 during ~~~~both OH and $^3C^*$ oxidations, indicating persistent formation of highly

786 oxygenated compounds including organic acids, such as formic acid and oxalic acid

787 (Sun et al., 2010). ~~Concentration~~Concentrations of ~~small~~ organic acids ~~rise~~

788 ~~over~~increased with photochemical ~~reaction~~reactions can ~~supported~~support this

789 assumption (data not shown). Note the f_{44} enhancement was much more significant for

790 $^3C^*$ oxidation (from 0.07 to 0.16) than direct photolysis (from 0.~~08~~07 to 0.12) and ~~~~OH

791 oxidation (from 0.07 to 0.13), consistent with the behaviors of its higher O/C and OSc.

792 The f_{43} value ~~actually~~decreased in the first stage (1-3 ~~h~~hours) and then increased at ~~the~~

793 later stages. The final f_{43} values ~~was~~were almost the same ~~with original solution.~~as those

794 of the initial solutions. As a result, all data points located outside the f_{44} vs. f_{43} space

795 ~~observed for ambient aerosol AMS dataset~~established by Ng et al. (2010~~),~~) for ambient

796 aerosols, owing to the relatively ~~lower~~low f_{43} values.

797 In summary, our results shown here demonstrate that aqueous phase eugenol

798 photochemical oxidation can generate highly oxygenated products and hence increase

799 the degree of oxygenation of overall SOA.

801

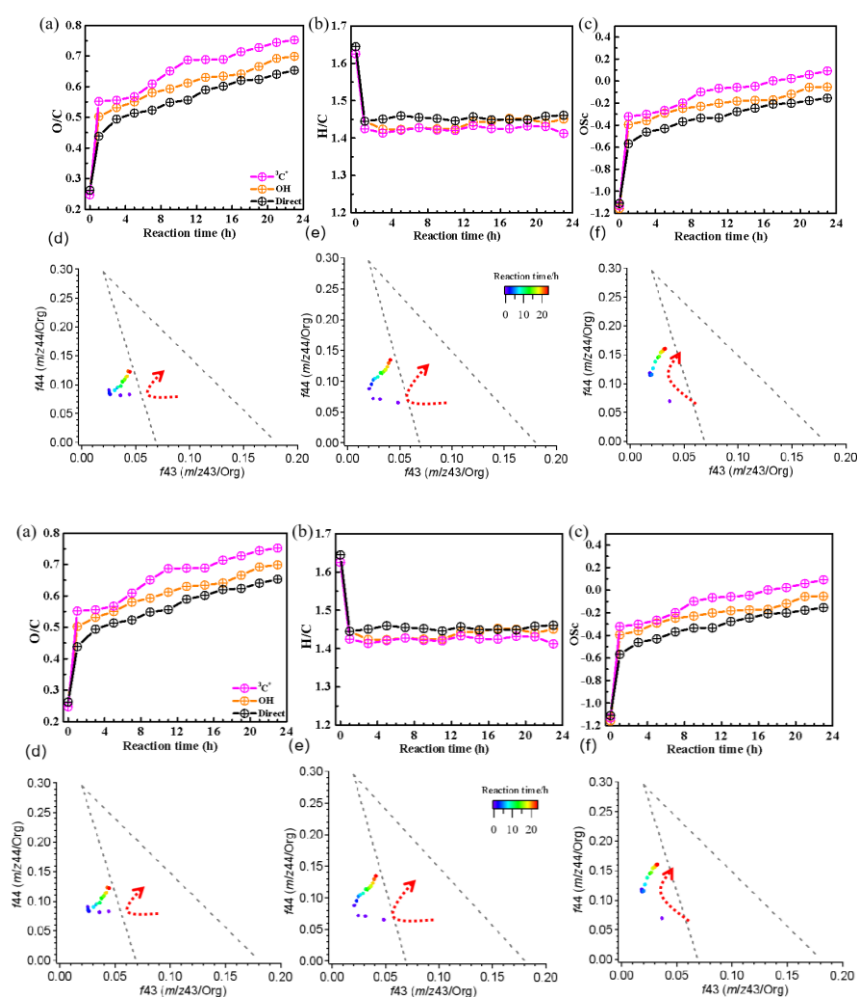802 **Figure 9.** Variations of elemental ratios of (a ~~c~~) ~~(~~) O/C, (b) H/C~~, O/C~~ and (c) the oxidation state

803 (OSc) as a function of reaction time, and the ~~"Triangle plot"~~f_{44} vs. f_{43} plots of ~~aqSOA (d f)~~reaction

804 products under (a) direct photolysis, (b) OH-initiated oxidation, and (c) ^{3}C*-initiated

805 ~~oxidations~~oxidation.

806 **3.6 Molecular characterization of reaction products and proposed reaction**

807 **mechanism**

808 **3.6.1 ~~Molecular characterization~~Major products identified by GC-MS**

809   SP-AMS was limited to probe bulk composition of low-volatility oxidation

810 products, thus the molecular-level characterization of products was performed by using

811 GC-MS here. The total ion chromatograph (TIC) of GC-MS on the solutions before

812 ~~irradiation~~illumination (0 ~~h~~hour) and at illumination times of 11 and 23 ~~h~~hours for the

813 $^3C^*$-initiated photooxidation is shown in Fig. S7. As shown in Fig.S7, eugenol (retention

814 time (RT) at 11.50 min) loss was more than 90% at 11 ~~h~~hours, which could be confirmed

815 by the experimental data reported in Section 3.1. Comparison of products at 11 ~~h~~hours

816 and 23 ~~h~~hours showed no significant difference. Similar to aqueous photochemical

817 oxidation ~~from~~with OH ~~oxidant~~ (Ye et al., 2020), a series of products were identified~~,~~

818 ~~including two additional compounds, 4-hydroxy-3-methoxy-mandelic acid (MW 198,~~

819 ~~RT=12.79 min) and 3,4-dihydroxy-, methyl ester-benzoicacid (MW 168, RT=13.39~~

820 ~~min).~~listed in Table 2. Except ~~for~~ 5-ally-3-methoxybenzene-1,2-diol (MW 180,

821 RT=12.59 min), the other eight products ~~have been~~were detected ~~in~~for both OH and

822 $^3C^*$-initiated ~~photooxidation.~~photooxidations. Some of them (Eugenol, DMB, product

823 1, 2, 5) were identified by using certified reference materials, some of them (product 3,

824 4, ~~9)~~identified by matching the NIST database, and others (product 6, 7, 8~~6, 7, 8, 9~~)

825 were inferred according to the molecular ion ~~peak~~peaks and fragments from GC-MS,

826 ~~combine with~~based on spectra from the NIST ~~matching results~~database (Stein, 2014)

827 and on the ~~start material &~~reactants and reaction conditions.

828   ~~——~~We also found 4-(1-hydroxypropyl)-2-methoxyphenol (product ~~1 (4-~~

829 ~~hydroxy-3-methoxyphenyl) with a carbonyl group~~8) was relatively abundant (Fig.S7),

830 suggesting functionalization ~~dominate. In summary, products~~might dominates as
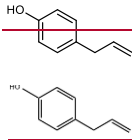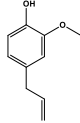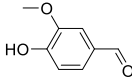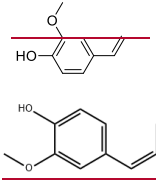
41
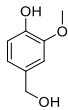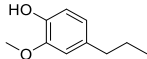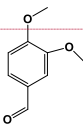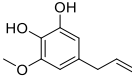
compared to oligomerization and fragmentation. Products were mainly from addition/elimination of hydroxyl (-OH), methoxyl (-OCH$_3$) to benzene ring or allyl group and further ~~oxidation~~oxidized to carbonyl or carboxyl compounds~~..~~. As suggested by Bonin et al~~.(~~. (2007), the OH-addition to the aromatic ring of phenol preferentially takes place at the ortho (48%) and the para (36%) positions, leading to the formation of OH-adduct product 6 (5-allyl-3-methoxybenzene-1,2-diol). Notably, dimers and ring-opening ~~product~~products were not observed, but ~~it~~they cannot be excluded since ~~it~~they would be probably out of the ~~range~~detection of GC-MS technique (Vione et al., 2014).

带格式的
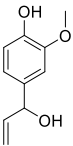
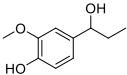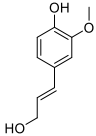840 **Table 2.** ~~Products~~Major reaction products identified via GC-MS ~~detection under ³C* system~~

	RT (min)	~~Material name~~Name*	~~Chemical~~Proposed chemical structure	Chemical formula	Nominal MW (g/mol)
Product 1	10.68	4-allylphenol		$C_9H_{10}O$	134
Precursor	11.50	Eugenol		$C_{10}H_{12}O_2$	164
Product 2	11.81	4-hydroxy-3-methoxybenzaldehyde		$C_8H_8O_3$	152
Product 3	12.06	(E)-2-methoxy-4-(prop-1-en-1-yl)phenol		$C_{10}H_{12}O_2$	164
Product 4	12.11	4-(hydroxymethyl)-2-methoxyphenol		$C_8H_{10}O_3$	154
Product 5	12.18	2-methoxy-4-propylphenol		$C_{10}H_{14}O_2$	166
Photosensitizer	12.29	3,4-dimethoxybenzaldehyde(DMB)		$C_9H_{10}O_3$	166
Product 6**	12.59	5-allyl-3-methoxybenzene-		$C_{10}H_{12}O_3$	180

43

		1,2-diol			
Product 7	12.65	4-(1-hydroxyallyl)-2-methoxyphenol		$C_{10}H_{12}O_3$	180
Product 8	12.79	4-(1-hydroxypropyl)-2-methoxyphenol		$C_{10}H_{14}O_3$	182
Product 9	12.91	(E)-4-(3-hydroxyprop-1-en-1-yl)-2-methoxyphenol		$C_{10}H_{12}O_3$	180

841 Note: *Precursor (eugenol) and triplet precursor (DMB) wasare also shown.

842 **This compound was only identified in $^3C^*$-oxidation solution.

3.6.2 Reaction mechanism

844 The reaction pathways of $^3C^*$-initiated photooxidation of eugenol are

845 demonstrated in Scheme 1 based on mainthe products identified by GC-MS. The

846 other intermediates and the potential pathwaypathways were inferred and proposed

847 according to the identified products and the reaction rationality from start material.the

848 starting reactant. To better describe pathwaysdepict the mechanism, DMB werewas

849 expressed as [RCHO] and eugenol as Ph-R for simplicity. First, [RCHO] absorbs light

850 and undergoundergoes excitation to $^1[RCHO]^*$, then experiences the intersystem

851 crossing (ISC) to form $^3[RCHO]^*$. The $^3[RCHO]^*$ can participate in latersubsequent

852 reactions via three channels. First, it can react with O_2 to form $^1O_2$ via energy transfer.

853 Secondly, it can becometransform to $[RCHO]^{\cdot-}$, subsequently reactreacts with O_2 to

854 generate $O_2^{\cdot-}$ via electron transfer, which can disproportionate to H_2O_2. The

44

decomposition of H_2O_2 can generate OH radical. Thirdly, the $^3[RCHO]^*$ can react with Ph-R to from [Ph-R•] via H-abstraction. The cleavage of [Ph-R•] to free radical segment (such as $CH_2CH•$ or $CH_3O•$) ~~take~~takes place, then an additional hydrogen transfer ~~would happen~~could occur, resulting in a 2H-addition to the new intermediate to form 4-allyl-phenol (product 1). Similarly, when the $CH_2CH•$ is lost from [Ph-R•], an addition of H_2O would happen on the new compound (product 4) and further oxidized to 4-hydroxy-3-methoxybenzaldehyde (product 2). Another possibility is the intermediate [Ph-R•] ~~could~~can resonate to several different isoelectronic species, the radical position ~~changing~~changes to aromatic ring or allyl group site, which would couple with HO• to form hydroxylated eugenol monomer (product 6, 7, 9 MW=180). Consequently, the isoelectronic species at allyl group site could also abstract a hydrogen to form isoeugenol (product 3 MW=164). Also, breakage of C=C into C-C and 2H-addition at allyl group site could form 2-methoxy-4-propyl-phenol (product 5, MW=166). Besides, the C=C breaking intermediate can couple with HO• to form 4-(1-hydroxypropyl)-2-methoxyphenol (product 8, MW=182). In conclusion, $^3C^*$ can directly oxidize eugenol to form SOA products or small molecular compounds, or indirectly oxidize eugenol via energy transfer, electron transfer, hydrogen abstraction, proton-coupled electron transfer or other radical chain reactions.

The organic groups, such as methoxy, allyl groups can be eliminated from aromatic ring, which then participate in photochemical reaction, resulting in generation of dimers, small organic acids, CO_2 and H_2O, ~~et al~~etc. Dimers previously reported from aqueous reaction of 4-methylsyringol with OH were not detected via GC-MS in the present work but dimer fragment ions ($C_{20}H_{22}O_4^+$) were detected by SP-AMS with trace amounts. Functionalization due to the additions of hydroxyl, carbonyl functional groups to the aromatic rings could account for the enhancement of light absorption at

带格式的: 突出显示

880 wavelength of 300-400 nm. ~~So, aqueous phase reactions of eugenol are likely an~~

881 ~~important source of BrC in the atmosphere, especially in regions of abundant biomass~~

882 ~~burning.~~ However, ~~some~~ polar high ~~molecular weight~~MW organic acids were not

883 detected likely due to the limitation of ~~analytical instrument of~~ GC-MS technique.

884

885

886
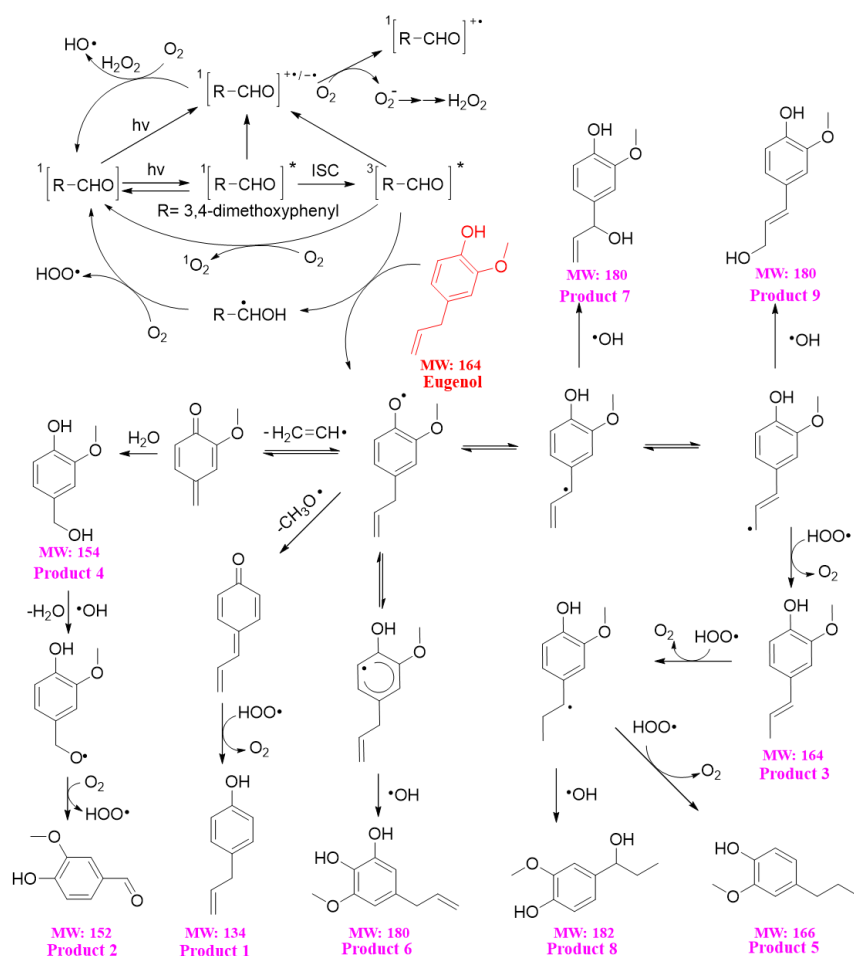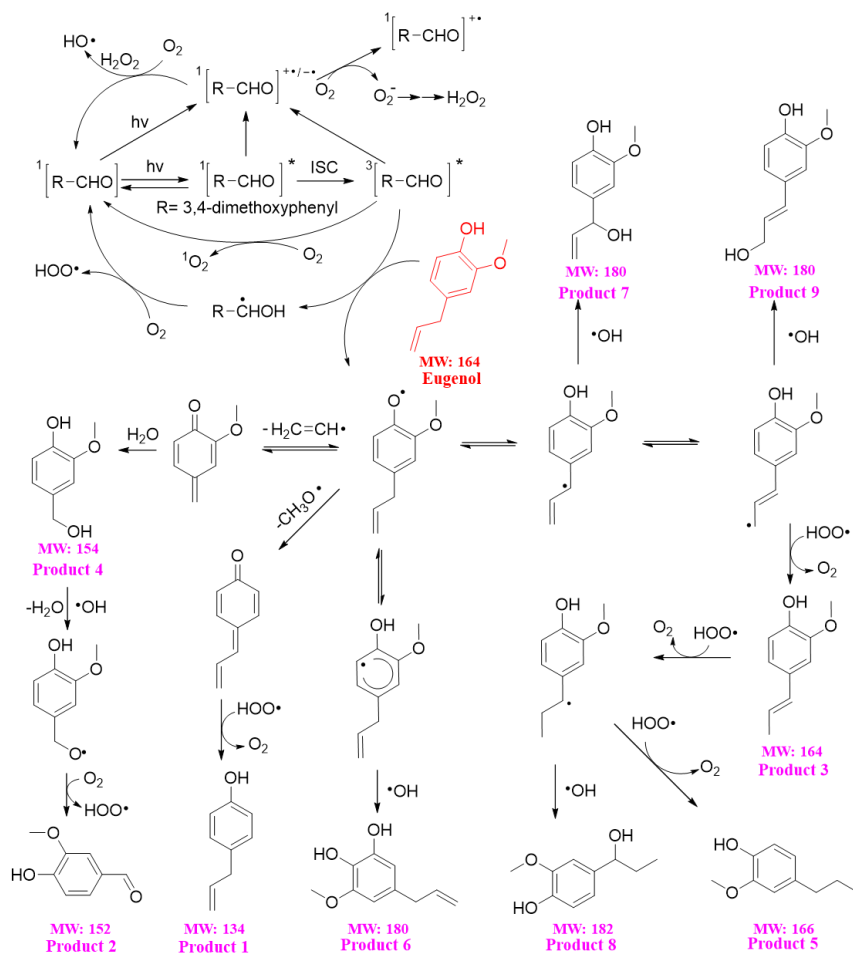
Scheme 1. Proposed ~~eugenol $^{3}C^{*}$ initiated~~ reaction mechanism_ _of $^{3}C^{*}$-initiated photooxidation of eugenol._ The red ~~text represents~~texts represent the ~~compounds~~products listed in Table ~~1~~2 identified by GC-MS.

3.7 Oxidative potential (OP) of reaction products

Previous laboratory studies (~~Chen et al., 2021;~~ Verma et al., 2015b; Xu et al., 2020) have confirmed that HULIS ~~are~~is a major ~~constituents~~constituent contributing to ROS-generation potential~~, and~~. As HULIS ~~were formed upon~~is an important fraction of the

products from aqueous photooxidation of eugenol in this work. ~~Based on above mentioned results,~~ (Fig. 7), here we ~~want to know whether or not there are some~~investigated the links between ~~DTT activity~~the OPs and ~~HULIS concentration. So, we detected the OP variation with~~ reaction ~~time~~products. The OP of ~~aqueous phase~~oxidation products can be represented by the consumption rate of DTT concentration per minute, defined as R_{DTT}. Figure 10a shows the DTT consumed mass (M_{DTT}) as a function of incubation times (0, 30, 60, 90, 120 and 150 min) for a triplicate sample (300 µM eugenol) and blank (ultrapure water). ~~As shown in Figure 10a,~~ M_{DTT} values for both blank and eugenol ~~sample~~ were proportional to incubation time, indicating that ROS-generating ~~substance~~substances in reaction solution ~~acts~~act only as catalyst and ~~was~~ itself was not consumed. The slopes ~~represented~~represent DTT consumption rates, which ~~were~~are also illustrated in Fig. ~~10a. According to Fig. 10a, we obtained average~~10a. Average R_{DTT0} (blank) ~~of~~was 0.31 µM/min and R_{DTT} for initial 300 µM eugenol (before experiment) ~~of~~was 0.52 µM/min. ~~According to other work, the~~Since self-oxidation of DTT might lead to the consumption of DTT in ultrapure water. ~~Final,~~ final DTT consumption rate ~~for reaction~~of reacted solution after photolysis was then blank-corrected by subtracting the average R_{DTT0}.

Figure 10b shows changes of blank-corrected R_{DTT} with photolysis time for direct photolysis, OH-initiated oxidation and $^3C^*$-initiated oxidation, respectively. The R_{DTT} value of $^3C^*$-~~initiated~~oxidation products increased quickly and reached the maximum (0.9) at 7 ~~h~~hours, then decreased slowly ~~but~~and its end value was ~~slower~~lower than that from OH-oxidation. The R_{DTT} value of OH-oxidation ~~system~~products on the other hand increased slowly and reached the maximum at 21 ~~h~~hours. The R_{DTT} value of products from direct photolysis ~~system~~increased continuously but also slowly to ~0.36 till the ~~termination~~end of oxidation. Nevertheless, we can see that the final R_{DTT} values were

48

all higher than that of initial eugenol, ~~providing evidence~~proving that aqueous ~~oxidation~~ phase processing can generate products ~~increases oxidative potential~~with higher OP, resulting in ~~adverse~~more health ~~effects~~hazards than the precursor ~~compounds especially for $^3C^*$-induced photolysis.~~does. The DTT consumption rates are comparable to ~~values by other researchers~~those using the same DTT method (Charrier and Anastasio, 2012; Lin and Yu, 2019). This finding further indicates the effectiveness of DTT method to represent OP. The ~~unexpected weaker~~<mark>weak</mark> correlation was found between HULIS concentration and R_{DTT} ~~value implied~~, implying that ~~oxidative potential~~OP was not only dependent ~~with~~upon HULIS. Moreover, HULIS with ~~different~~diverse molecular ~~structure~~structures also ~~exhibited~~exhibit different ROS-generation ~~potential~~potentials (Kramer et al., 2016), ~~as a result, absolute concentration of~~therefore the HULIS ~~did~~as an ensemble may not ~~correlated~~correlate well with OP.

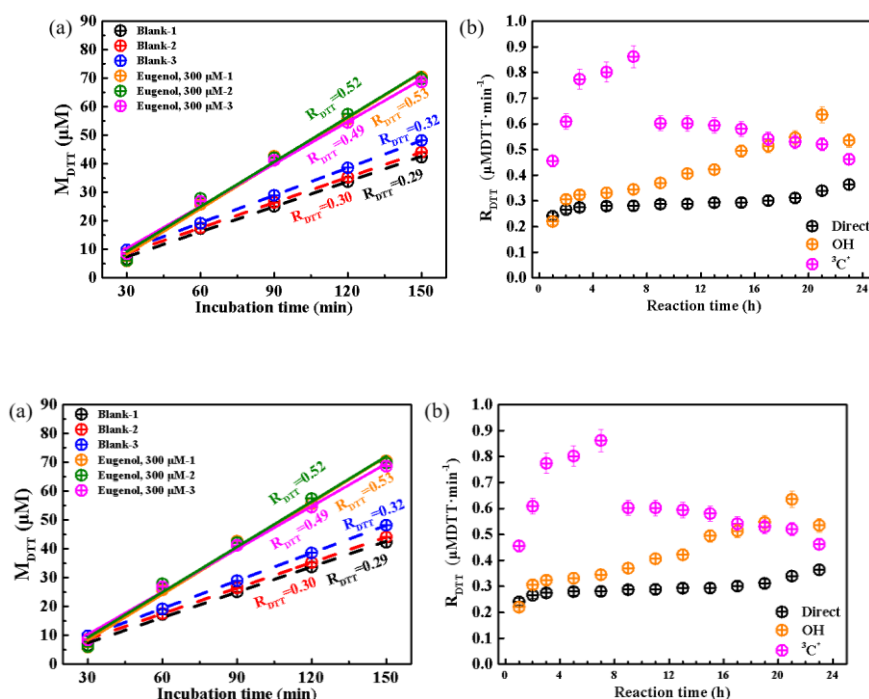**Figure 10.** (a) DTT ~~consumption~~consumed mass versus incubation ~~time~~times for ~~blanks~~blank (ultrapure water) and 300 μM eugenol solutions in a ~~triplicate~~ ~~experiments~~, and (b) blank-corrected DTT consumption ~~rate~~rates versus reaction time for direct photolysis, OH-initiated oxidation and $^3C^*$-*-induced oxidation.

4. Atmospheric implications

The high mass yields of aqueous-phase photooxidation of eugenol (exceeding 100% after 23 hours of illumination) studied here are similar or even higher than those previously reported yields of a number of phenolic compounds (e.g., Smith et al., 2014, 2015, 2016; Ma et al., 2021), which re-emphasizes the importance of biomass burning (BB) to SOA budget (Gilardoni et al., 2016), particularly in regions or periods with significant BB activities. Compared to simple phenols (such as syringol) that are only present in cloud/fog waters, the highly substituted phenols are able to significantly partition into aerosol water too (Ma et al., 2021). Since the highly substituted phenols can take up roughly 30−45% of total phenols emitted from wood burning (Schauer et al., 2001), our results further imply that aqueous production of SOA from BB emissions can not only occur in fog/cloud conditions, but also in common humid weather conditions, highlighting the general importance of aqueous oxidation pathway to SOA.

Our study here used 300 μM H_2O_2 and 15 μM DMB as sources of OH and $^3C^*$, and $^3C^*$-mediated oxidation appeared to be faster than OH-initiated oxidation of eugenol. Of course, whether or not $^3C^*$ is more important than OH in real atmosphere depends upon their concentrations. OH and $^3C^*$ are difficult to measure and concentrations vary greatly in real atmospheric samples. Herrmann et al. (2010) estimated an average OH level of 0.35×10^{-14} M in urban fog water; Kaur and Anastasio (2018) measured $^3C^*$ concentration to be $(0.70\text{-}15) \times 10^{-14}$ M, 10-100 times higher than co-existing OH in

958 ambient fog waters; Kaur et al. (2019) determined both OH and $^3C^*$ concentrations in

959 PM extracts, OH steady-state concentration was $4.4(\pm2.3) \times 10^{-16}$ M, similar to its level

960 in fog, cloud and rain, while $^3C^*$ concentration was $1.0(\pm0.4) \times 10^{-13}$ M, a few hundred

961 times higher than OH and nearly double its average value in fog. Therefore, together

962 with these measurements, our findings signify a likely more important role of $^3C^*$ than

963 OH in aqueous-phase (especially aerosol water) reactions. In addition, quenching

964 experiments reveal that O_2 can inhibit eugenol degradation by effectively scavenging

965 $^3C^*$ radical while it can promote degradation by fostering radical chain reactions in OH-

966 induced oxidation, which offer insights to control of reaction pathways by regulating

967 the ROS generations; of course, such operation calls for application of highly sensitive

968 EPR method.

969 Eugenol has a strong light absorption peak around 280 nm, therefore it can

970 photolyze itself, and addition of OH or other photosensitizers ($^3C^*$) can gradually

971 diminish its light absorption around 280 nm, but increase the absorption in visible light

972 range (>300 nm). In the meantime, HULIS was generated continuously, and GC-MS

973 identified a number of high MW organic products, in line with those detected in earlier

974 aqueous photooxidation of phenolic compounds (Jiang et al., 2021; Misovich et al.,

975 2021; Tang et al., 2020; Yu et al., 2014). Overall, our work demonstrates that aqueous

976 oxidation of BB emissions is a source of BrC, and this BrC may act as photosensitizer

977 to oxidize other species; a portion of this BrC might be HULIS, and some high MW

978 aromatic compounds are a subset of this HULIS. However, a recent study by Wang et

979 al. (2021) shows that fossil foil derived OA (FFOA) can be an effective precursor of

980 aqSOA, but the aqSOA became less light-absorbing than the FFOA. Aqueous oxidation

981 of 4-nitrophenol with OH can lead to a photobleaching effect too (Witkowski et al.,

982 2022). These contrasting results indicate that contribution of aqueous oxidation to BrC

51

is largely dependent upon the precursors; molecular structures of major chromophores, changes of the structures upon oxidation as well as their interplay with light absorptivity should be carefully investigated to achieve a full understanding of the impacts of aqueous processing on air quality, radiative forcing and climate change.

Investigations on the OPs of reaction products from eugenol photooxidation in all three conditions show that aqueous processing can produce more toxic products than its precursor. This result is in agreement with our previous work on resorcinol, hydroquinone and methoxyhydroquinone (Ou et al., 2021).

4. Conclusions and atmospheric implication

This work systematically investigated the aqueous phase photochemistry of eugenol under both OH and $^3C^*$ radicals. Comprehensive analysis of the reaction kinetics, chemical and optical characteristics as well as oxidative potential of the products was conducted. Our results showed eugenol loss more in $^3C^*$ initiated photooxidation. With the combination of quenching experiments, ESR method and different saturated gas experiments, it can be concluded that both $^3C^*$ and $^1O_2$ were responsible for eugenol degradation in $^3C^*$ initiated oxidation, while $O_2^{\cdot-}$ played crucial role in OH initiated reaction. Interestingly, O_2 can inhibit eugenol degradation by effectively quenching $^3C^*$ radical while it can promote degradation by foster radical chain reactions in OH induced reaction. Above experimental results also offered us an insight into the degradation mechanism of eugenol involved with ROS. It can also enlighten the readers how to control reaction pathway via regulating the ROS generation during aqueous reaction. Surely, to elucidate the role of each ROS, we should investigate the time-dependent variation of generated ROS via high-sensitivity EPR.

Significant absorption enhancement over the range of near UV region (300-400 nm)

1007 pointed out the continuous generation of BrC (i.e., HULIS). Direct HULIS

1008 concentration determination confirmed that HULIS was formed continuously over the

1009 course of reaction. Consequently, these light-absorbing products contribute to

1010 fluorescence at EX of 400-500 nm. GC-MS analysis confirmed the formation of high

1011 molecular weight multi-functional organic compounds, which has also been reported

1012 previously in similar aqueous phenolic photochemical experiments (Jiang et al., 2021;

1013 Misovich et al., Although more studies on a broad spectrum of atmospherically relevant

1014 species and multiple indicators of toxicity are clearly needed, our findings here

1015 underscore the potential of aqueous processing on the enhancement of particle toxicity.

1016 Considering high PM concentration is often accompanied with cold and humid weather

1017 conditions, the additional adverse health effects caused by aqueous oxidation may

1018 amplify the health hazards of PM pollution.

5 Conclusions

1020   This study comprehensively investigated the aqueous photooxidation of eugenol

1021 upon direct photolysis and attacks by OH and $^3C^*$ radicals. By using a suite of

1022 techniques, the decay kinetics of eugenol, chemical, optical properties as well as

1023 toxicity of reaction products were systematically studied. The first-order photolysis rate

1024 constants followed the order of $^3C^*$>OH >direct photolysis (300 μM H_2O_2 and 15 μM

1025 DMB as sources of OH and $^3C^*$). Further quenching experiments on different ROS

1026 during $^3C^*$-mediated oxidation showed that $^3C^*$ was the major contributor, followed by

1027 $^1O_2$, $O_2^{\cdot-}$ and OH; $O_2^{\cdot-}$ played a more important role than OH during OH-initiated

1028 oxidation. Photolysis rate constants under saturated O_2, air and N_2 followed the order

1029 of $k_{O_2} > k_{Air} > k_{N_2}$ for both direct photolysis and OH-initiated oxidation, but changed to

1030 $k_{Air} > k_{N_2} > k_{O_2}$ for $^3C^*$-mediated oxidation. O_2 appeared to be a scavenger of $^3C^*$

53

therefore suppressing $^3C^*$ oxidation while it could promote generation of OH thus accelerate OH-mediated oxidation. pH and DO levels both decreased during oxidation, indicating formation of acids and a certain role of DO in oxidation.

Eugenol itself can absorbs lights significantly around 280 nm, and aqueous oxidation gradually decrease this absorption of UV light but enhanced the absorbance in the visible light range (mainly 300-400 nm), indicative of the generation of BrC species. These species were likely linked with HULIS, as HULIS concentration increased during the course of oxidation, in particular for the initial stage of $^3C^*$-mediated reactions. The final mass yields of reaction products (after 23 hours of irradiation) were 140.1%, 144.9% and 196.5% for direct photolysis, OH-oxidation and $^3C^*$-oxidation, respectively. Oxidation degrees of the products increased continuously with the illumination time, indicating persistent formation of highly oxygenated compounds, especially during $^3C^*$-mediated reactions. Molecular characterization by GC-MS identified a series of oxygenated compounds, allowing us to propose the detailed oxidation mechanism. Functionalization appeared to be a dominant pathway to form the observed species.

DTT method was used to assess OPs of the reaction products. The end products in all three cases showed higher DDT consumption rates than that of the precursor; products from $^3C^*$-oxidation showed particularly fast increase in the first few hours of reactions. This result demonstrates that species that are more toxic than its precursors could be produced upon aqueous oxidation, indicative of the potential toxic effects induced by aqueous processing. Overall, by using eugenol as a model compound of BB emissions, our findings highlight the importance of aqueous oxidation of BB emissions to SOA formation, its potentially important role in affecting radiative balance and climate through formation of BrC, as well as possible additional adverse health effects.

54

Such effects should be considered in air quality or climate models to better assess the influence of BB emissions.

2021; Tang et al., 2020; Yu et al., 2014). Overall, our work shows that SVOCs-aqSOA is an important source of BrC, therefore aqueous chemical processes may play a role in aerosol light absorption, radiative forcing, as well as climate change. In-depth molecular-level characterization or functional groups with respect to HULIS should be carried out in the future study. Except for influencing the radiative balance of atmosphere, the aqueous photoreaction of phenolic compounds may contribute to the formation of small volatile organics, i.e., dicarboxylic acid, that are emitted in the gas phase and further participate in the SOA formation.

Both DTT consumption rate and EEM have been applied for the investigation of atmospheric aerosol, but not for aqueous-phase photoreaction. Our present work for the first time showed that DTT consumption rate of products was in the order of $^3C^*$>OH>direct, suggesting that oxidative stress of products was higher in $^3C^*$-initiated photolysis process. Additionally, new fluorescence peak at Ex/EM=250/400-500nm in EEM fluorescence spectra suggesting the formation of HULIS. In future, the relationship between EEM components and chemical structure of HULIS must be studied statistically via advanced analysis method. Considering that different chemical species and concentrations of them involved can change reaction pathway leading to different products, optical and toxic investigations of aqueous phase reaction products must be performed under a wide variety of S/IVOCs as precursor.

Eugenol emitted in significant quantities by wood combustion undergoes rapid aqueous phase oxidation to produce aqSOA. High SOA yields (exceed 100%) from aqueous-phase photochemical reactions of eugenol in our work and reported high yields (25-50%) from OH-initiated gas phase chemistry further demonstrated that phenolic

~~compounds are most significant SOA precursors. Results from highly substituted phenols (has high Henry's law constants) with $^3C*$ oxidant also showed aqSOA mass yields from triplet reaction was significant under high aerosol liquid water conditions (Ma et al., 2021). Since the highly substituted phenols measured by Schauer et al.(2001) are abundant, together making up roughly 30–45% of total phenols emitted from wood burning, contribution from $^3C*$ initiated aqueous phase reaction to SOA should be paid more attention. Both OS_C and O/C ratio of aqSOA are higher than those of precursor in this AMS-based study, indicating formation of highly oxidized products (i.e., carboxylic acid), which also showed the occurrence of oxygenation pathways such as electrophilic addition of OH radical to the aromatic ring. Surely, we should characterized in more detail the molecular-level chemical and light-absorbing components of SOA in order to elucidate the mechanisms responsible for its formation.~~

Data availability. The data in this study are available from the authors upon request (bess_ye@jsut.edu.cn or ~~caxinra@163.covm)~~caxinra@163.com)

Supplement. The supplement related to this article is available on line at:

Author Contributions: XDL, YT, LWZ, SSM, SPL, ZZZ and NS conducted the experiments. XDL and YT analyzed the data. XDL and ZLY prepared and wrote the paper with contributions from all co-authors. ZLY and XLG reviewed and commented on the paper.

Competing interests. The authors declare that they have no conflict of interest.

References

Alam, M. S., Delgado-Saborit, J. M., Stark, C., and Harrison, R. M.: Using atmospheric measurements of PAH and quinone compounds at roadside and urban background sites to assess sources and reactivity, Atmos. Environ., 77(3), 24-35, https://doi.org/10.1016/j.atmosenv.2013.04.068, 2013.

Alegría, A. E., Ferrer, A., Santiago, G., Sepúlveda, E., and Flores, W.: Photochemistry of water-soluble quinones. Production of the hydroxyl radical, singlet oxygen and the superoxide ion, J. Photochem. Photobiol. Chem., 127, 57-65, https://doi.org/10.1016/S1010-6030(99)00138-0, 1999.

Arakaki, T., Anastasio, C., Kuroki, Y., Nakajima, H., Okada, K., Kotani, Y., Handa, D., Azechi, S., Kimura, T., Tsuhako, A., and Miyagi, Y.: A general scavenging rate constant for reaction of hydroxyl radical with organic carbon in atmospheric waters, Environ. Sci. Technol., 47, 8196-8203, https://doi.org/10.1021/es401927b, 2013.

1132 Aryal, R., Lee, B. K., Beecham, S., Kandasamy, J., Aryal, N., and Parajuli, K.: Characterisation of road

1133   dust organic matter as a function of particle size: A PARAFAC Approach, Water Air Soil Poll.;

1134   226, https://doi.org/10.1007/s11270-014-2289-y, 2015.

1135 Bari, M, A, Baumbach, G., Kuch, B., and Scheffknecht, G.. Wood smoke as a source of particle-

1136   phase organic compoundsin residential areas, Atmos. Environ., 43, 4722-4732,

1137   https://doi.org/10.1016/j.atmosenv.2008.09.006, 2009.

1138 Barzaghi, P. and Herrmann, H.: A mechanistic study of the oxidation of phenol by OH/NO2/NO$_3$ in

1139   aqueous solution, Phys. Chem. Chem. Phys., 4, 3669-3675,

1140   https://doi.org/10.1039/B201652D, 2002.

1141 Barsotti, F., Ghigo, G., and Vione, D. Computational assessment of the fluorescence emission of

1142   phenol oligomers: A possible insight into the fluorescence properties of humic-like Substances

1143   (HULIS), J. Photochem. Photobio. A, 315, 87-93,

1144   https://doi.org/10.1016/j.jphotochem.2015.09.012, 2016.

1145 Barzaghi, P. and Herrmann, H.: A mechanistic study of the oxidation of phenol by OH/NO2/NO$_3$ in

1146   aqueous solution, Phys. Chem. Chem. Phys., 4, 3669-3675,

1147   https://doi.org/10.1039/B201652D, 2002.

1148 Bianco, A., Minella, M., De Laurentiis, E., Maurino, V., Minero, C., and Vione, D. Photochemical

1149   generation of photoactive compounds with fulvic-like and humic-like fluorescence in aqueous

1150   solution, Chemosphere, 111, 529-536, https://dx.doi.org/10.1016/j.chemosphere.2014.04.035,

1151   2014.

1152 Bonin, J., Janik, I., Janik, D. and Bartels, D. M.: Reaction of the hydroxyl radical with phenol in water

1153   up to supercritical conditions, J. Phys. Chem. A, 111(10), 1869-1878,

1154   https://doi.org/10.1021/jp0665325, 2007.

1155 Canagaratna, M. R., Jimenez, J. L., Kroll, J. H., Chen, Q., Kessler, S. H., Massoli, P., Hildebrandt Ruiz,

1156   L., Fortner, E., Williams, L. R., Wilson, K. R., Surratt, J. D., Donahue, N. M., Jayne, J. T., and

1157   Worsnop, D. R.: Elemental ratio measurements of organic compounds using aerosol mass

1158   spectrometry: characterization, improved calibration, and implications, Atmos. Chem. Phys.,

1159   15, 253-272, https://doi.org/10.5194/acp-15-253-2015, 2015.

1160 Chang, J. L., and Thompson, J. E.: Characterization of colored products formed during irradiation of

1161   aqueous solutions containing H$_2$O$_2$ and phenolic compounds, Atmos. Environ., 44, 541-551,

带格式的: 默认段落字体

https://doi.org/10.1016/j.atmosenv.2009.10.042, 2010.

Charrier, J. G., and Anastasio, C.: On dithiothreitol (DTT) as a measure of oxidative potential for ambient particles: evidence for the importance of soluble transition metals, Atmos. Chem. Phys. 12, 9321-9333, https://doi.org/10.5194/acp-12-9321-2012, 2012.

Chen, H., Ge, X., Ye, Z.: Aqueous-phase secondary organic aerosol formation via reactions with organic triplet excited states—a short review. Curr. Pollut. Rep., 4, 8-12, https://doi.org/10.1007/s40726-018-0079-7, 2018.

Chen, Q., Ikemori, F., and Mochida, M.: Light Absorption and excitation-emission fluorescence of urban organic aerosol components and their relationship to chemical structure, Environ. Sci. Technol., 50, 10859-10868, https://doi.org/10.1021/acs.est.6b02541, 2016a.

Chen, Q., Miyazaki, Y., Kawamura, K., Matsumoto, K., Coburn, S., Volkamer, R., Iwamoto, Y., Kagami, S., Deng, Y., Ogawa, S., Ramasamy, S., Kato, S., Ida, A., Kajii, Y., and Mochida, M.: Characterization of chromophoric water-soluble organic matter in urban, forest, and marine aerosols by HR-ToF-AMS analysis and excitation-emission matrix spectroscopy, Environ. Sci. Technol., 50, 10351-10360, https://doi.org/10.1021/acs.est.6b01643, 2016b.

Chen, Q., Wang, M., Wang, Y., Zhang, L., Li, Y., and Han, Y.: Oxidative potential of water-soluble matter associated with chromophoric substances in $PM_{2.5}$ over Xi'an, China, Environ. Sci. Technol., 53, 8574-8584, https://doi.org/10.1021/acs.est.9b01976, 2019.

Chen, Y., Li, N., Li, X., Tao, Y., Luo, S., Zhao, Z., Ma, S., Huang, H., Chen, Y., Ye, Z., and Ge, X.: Secondary organic aerosol formation from $^3C^*$-initiated oxidation of 4-ethylguaiacol in atmospheric aqueous-phase, Sci. Total. Environ., 723, 137953, https://doi.org/10.1016/j.scitotenv.2020.137953, 2020.

Cho, A. K., Sioutas, C., Miguel, A. H., Kumagai, Y., Schmitz, D. A., Singh, M., Eiguren-Fernandez, A., and Froines, J. R.: Redox activity of airborne particulate matter at different sites in the Los Angeles Basin, Environ. Res., 99, 40-7, https://doi.org/10.1016/j.envres.2005.01.003, 2005.

De Laurentiis, E., Sur, B., Pazzi, M., Maurino, V., Minero, C., Mailhot, G., Brigante, M., and Vione, D.: Phenol transformation and dimerisation, photosensitised by the triplet state of 1-nitronaphthalene: A possible pathway to humic-like substances (HULIS) in atmospheric waters, Atmos. Environ., 70, 318-327, https://doi.org/10.1016/j.atmosenv.2013.01.014, 2013.

Dou, J., Lin, P., Kuang, B. Y., and Yu, J.: Reactive oxygen species production mediated by humic-like

1192 substances in atmospheric aerosols: enhancement effects by pyridine, imidazole, and their

1193 derivatives, Environ. Sci. Technol., 49(11), 6457-6465, https://doi.org/10.1021/es5059378,

1194 2015.

1195 Ervens, B., Turpin, B. J., and Weber, R. J.: Secondary organic aerosol formation in cloud droplets and

1196 aqueous particles (aqSOA): a review of laboratory, field and model studies, Atmos. Chem. Phys.,

1197 11, 11069-11102, https://doi.org/10.5194/acp-11-11069-2011, 2011.

1198 Fang, T., Verma, V., Bates, J. T., Abrams, J., Klein, M., Strickland, M. J., Sarnat, S. E., Chang, H. H.,

1199 Mulholland, J. A., Tolbert, P. E., Russell, A. G., and Weber, R. J.: Oxidative potential of ambient

1200 water-soluble $PM_{2.5}$ in the southeastern United States: contrasts in sources and health

1201 associations between ascorbic acid (AA) and dithiothreitol (DTT) assays, Atmos. Chem. Phys.,

1202 16, 3865-3879, https://doi.org/10.5194/acp-16-3865-2016, 2016.

1203 Faust, J. A., Wong, J. P., Lee, A. K., and Abbatt, J. P.: Role of aerosol liquid water in secondary organic

1204 aerosol formation from volatile organic compounds, Environ. Sci. Technol., 51, 1405-1413,

1205 https://doi.org/10.1021/acs.est.6b04700, 2017.

1206 Ge, X., Li, L., Chen, Y., Chen, H., Wu, D., Wang, J., Xie, X., Ge, S., Ye, Z., Xu, J., and Chen, M. Aerosol

1207 characteristics and sources in Yangzhou, China resolved by offline aerosol mass spectrometry

1208 and other techniques. Environ. Pollut., 225, 74-85, https://doi.org/

1209 10.1016/j.envpol.2017.03.044, 2017.

1210 Graber, E. R., and Rudich, Y.: Atmospheric HULIS: how humic-like are they? A comprehensive and

1211 critical review, Atmos. Chem. Phys., 6, 729-753, https://doi.org/10.5194/acp-6-729-2006,

1212 2006.

1213 George, K. M., Ruthenburg, T. C., Smith, J., Yu, L., Zhang, Q., Anastasio, C., and Dillner, A. M.: FT-IR

1214 quantification of the carbonyl functional group in aqueous-phase secondary organic aerosol from

1215 phenols, Atmos. Environ., 100, 230-237, https://doi.org/10.1016/j.atmosenv.2014.11.011, 2015.

1216 Gilardoni, S., Massoli, P., Paglione, M., Giulianelli, L., Carbone, C., Rinaldi, M., Decesari, S., Sandrini,

1217 S., Costabile, F., Gobbi, G. P., Pietrogrande, M. C., Visentin, M., Scotto, F., Fuzzi, S., and

1218 Facchini, M. C.: Direct observation of aqueous secondary organic aerosol from biomass-

1219 burning emissions, Proc. Natl. Acad. Sci. USA., 113, 10013-810018,

1220 https://doi.org/10.1073/pnas.1602212113, 2016.

1221 Gligorovski, S., Strekowski, R., Barbati, S., and Vinoe, D.: Environmental implications of hydroxyl

1222   radicals (OH), Chem. Rev., 115(24), 13051-13092, https://doi.org/10.1021/cr500310b, 2015.

1223 Graber, E. R., and Rudich, Y.: Atmospheric HULIS: how humic-like are they? A comprehensive and

1224   critical review, Atmos. Chem. Phys., 6, 729-753, https://doi.org/10.5194/acp-6-729-2006,

1225   2006.

1226 Guo, Y., Zhang, Y., Yu, G., and Wang, Y., Revisiting the role of reactive oxygen species for pollutant

1227   abatement during catalytic ozonation: the probe approach versus the scavenger approach, Appl.

1228   Catal. B Environ., 280, 119418, https://doi.org/10.1016/j.apcatb.2020.119418, 2021.

1229 Hawthorne, S.B., Krieger M.S., Miller D.J., and Mathiason M.B. Collection and quantitation of

1230   methoxylated phenol tracers for atmospheric pollution from residential wood stoves, Environ. Sci.

1231   Technol., 23,470-475, https://doi.org/10.1021/es00181a013, 1989.

1232 He, L., Schaefer, T., Otto, T., Kroflic, A., and Herrmann, H.: Kinetic and theoretical study of the

1233   atmospheric aqueous-phase reactions of OH radicals with methoxyphenolic compounds, J. Phys.

1234   Chem. A, 123, 7828-7838, https://doi.org/10.1021/acs.jpca.9b05696, 2019.

1235 Herrmann, H.: Kinetics of aqueous phase reaction relevant for atmospheric chemistry, Chem. Rev., 103,

1236   4691-4716, https://doi.org/10.1021/cr020658q, 2003.

1237 Herrmann, H., Hoffmann, D., Schaefer, T., Bräuer, P. and Tilgner, A.: Tropospheric aqueous-phase free-

1238   radical chemistry: Radical sources, spectra, reaction kinetics and prediction tools.

1239   ChemPhysChem, 11, 3796-3822, https://doi.org/10.1002/cphc.201000533, 2010.

1240 Herrmann, H., Schaefer, T., Tilgner, A., Styler, S. A., Weller, C., Teich, M. and Otto, T.: Tropospheric

1241   aqueous-phase chemistry: kinetics, mechanisms, and its coupling to a changing gas phase,

1242   Chem. Rev., 115(10), 4259-4334, https://doi.org/10.1021/cr500447k, 2015.

1243 Hong, J., Han, B., Yuan, N., and Gu, J.: The roles of active species in photo-decomposition of organic

1244   compounds by microwave powered electrodeless discharge lamps, J. Environ. Sci. (China), 33,

1245   60-868, https://doi.org/10.1016/j.jes.2014.12.016, 2015.

1246 Huang, D., Zhang, X., Chen, Z. M., Zhao, Y., and Shen, X. L.: The kinetics and mechanism of an aqueous

1247   phase isoprene reaction with hydroxyl radical, Atmos. Chem. Phys., 11, 7399-7415,

1248   https://doi.org/10.5194/acp-11-7399-2011, 2011.

1249 Huang, D., Zhang, Q., Cheung, H. H. Y., Yu, L., Zhou, S., Anastasio, C., Smith, J. D., and Chan, C. K.:

1250   Formation and evolution of aqSOA from aqueous-phase reactions of phenolic carbonyls:

1251   comparison between ammonium sulfate and ammonium nitrate solutions, Environ. Sci.

Technol., 52, 9215-9224, https://doi.org/10.1021/acs.est.8b03441, 2018.

Huo, Y., Guo, Z., Li, Q., Wu, D., Ding, X., Liu, A., Huang, D., Qiu, G., Wu, M., Zhao, Z., Sun, H., Song, W., Li, X., Chen, Y., Wu, T., and Chen, J. Chemical fingerprinting of HULIS in particulate matters emitted from residential coal and biomass combustion, Environ. Sci. Technol., 55, 3593-3603. https://doi.org/10.1021/acs. est.0c08518, 2021.

Jiang, W., Misovich, M. V., Hettiyadura, A. P. S., Laskin, A., McFall, A. S., Anastasio, C., and Zhang, Q.: Photosensitized reactions of a phenolic carbonyl from wood combustion in the aqueous phase-chemical evolution and light absorption properties of aqSOA, Environ. Sci. Technol., 55, 5199-5211, https://doi.org/10.1021/acs.est.0c07581, 2021.

Kaur, R., and Anastasio, C.: First measurements of organic triplet excited states in atmospheric waters, Environ. Sci. Technol., 52, 5218-5226, https://doi.org/10.1021/acs.est.7b06699, 2018.

Kaur, R., Labins, J. R., Helbock, S. S., Jiang, W., Bein, K. J., Zhang, Q., and Anastasio, C.: Photooxidants from brown carbon and other chromophores in illuminated particle extracts, Atmos. Chem. Phys., 19, 6579-6594, https://doi.org/10.5194/acp-19-6579-2019, 2019.

Kramer, A.J., Rattanavaraha, W., Zhang, Z., Gold, A., Surratt, J.D., and Lin, Y.-H. Assessing the oxidative potential of isoprene-derived epoxides and secondary organic aerosol, Atmos. Environ., 130, 211-218, https://dx.doi.org/10.1016/j.atmosenv.2015.10.018, 2016.

Kroll, J. H., Donahue, N. M., Jimenez, J. L., Kessler, S. H., Canagaratna, M. R., Wilson, K. R., Altieri, K. E., Mazzoleni, L. R., Wozniak, A. S., Bluhm, H., Mysak, E. R., Smith, J. D., Kolb, C. E., and Worsnop, D. R.: Carbon oxidation state as a metric for describing the chemistry of atmospheric organic aerosol, Nat. Chem., 3, 133-9, https://doi.org/10.1038/nchem.948, 2011.

Laurentiis, E. D., Socorro, J., Vione, D., Quivet, E., Brigante, M., Mailhot, G., Wortham, H., and Gligorovski, S.: Phototransformation of 4-phenoxyphenol sensitised by 4-carboxybenzophenone: evidence of new photochemical pathways in the bulk aqueous phase and on the surface of aerosol deliquescent particles, Atmos. Environ., 8, 569-578, https://doi.org/10.1016/j.atmosenv.2013.09.036, 2013.

Lee, A. K. Y., Hayden, K. L., Herckes, P., Leaitch, W. R., Liggio, J., Macdonald, A. M., and Abbatt, J. P. D.: Characterization of aerosol and cloud water at a mountain site during WACS 2010: secondary organic aerosol formation through oxidative cloud processing, Atmos. Chem. Phys., 12, 7103-7116, https://doi.org/10.5194/acp-12-7103-2012, 2012.

Leenheer, J. A., and Croue, J. P. Characterizing aquatic dissolved organic matter, Environ. Sci. Technol., 37, 18A-26A, https://doi.org/10.1021/es032333c, 2003.

Li, F., Tsona, N. T., Li, J., and Du, L.: Aqueous-phase oxidation of syringic acid emitted from biomass burning: formation of light-absorbing compounds, Sci. Total Environ., 765, 144239, https://doi.org/10.1016/j.scitotenv.2020.144239, 2021.

Li, Y. J., Huang, D. D., Cheung, H. Y., Lee, A. K. Y., and Chan, C. K.: Aqueous-phase photochemical oxidation and direct photolysis of vanillin-a model compound of methoxy phenols from biomass burning, Atmos. Chem. Phys., 14, 2871-2885, https://doi.org/10.5194/acp-14-2871-2014, 2014.

Lim, Y. B., Tan, Y., Perri, M. J., Seitzinger, S. P., and Turpin, B. J.: Aqueous chemistry and its role in secondary organic aerosol (SOA) formation, Atmos. Chem. Phys., 10, 10521-10539, https://doi.org/10.5194/acpd-10-14161-2010, 2010.

Lin, M., and Yu, J. Z.: Dithiothreitol (DTT) concentration effect and its implications on the applicability of DTT assay to evaluate the oxidative potential of atmospheric aerosol samples, Environ. Pollut., 251, 938-944, https://doi.org/10.1016/j.envpol.2019.05.074, 2019.

~~Liu, C.G., Liu, Y.C., Chen, T.Z., Liu, J., and He, H. Rate constant and secondary organic aerosol formation from the gas-phase reaction of eugenol with hydroxyl radicals, Atmos. Chem. Phys., 19, 2001-2013, https://doi.org/10.5194/acp-19-2001-2019, 2019.~~

Ma, L., Guzman, C., Niedek, C., Tran, T., Zhang, Q. and Anastasio, C.: Kinetics and mass yields of aqueous secondary organic aerosol from highly substituted phenols reacting with a triplet excited state, Environ. Sci. Technol., 55(9), 5772-5781, doi:10.1021/acs.est.1c00575, 2021.

Ma, Y., Cheng, Y., Qiu, X., Cao, G., Kuang, B., Yu, J.Z., and Hu, D. Optical properties, source apportionment and redox activity of Humic-Like Substances (HULIS) in airborne fine particulates in Hong Kong, Environ. Pollut., 255,113087, https://doi.org/10.1016/j.envpol.2019.113087, 2019.

Mabato, B. R. G., Lyu, Y., Ji, Y., Li, Y., Huang, D., Li, X., Nah, T., Lam, C. H., and Chan, C. K.: Aqueous secondary organic aerosol formation from the direct photosensitized oxidation of vanillin in the absence and presence of ammonium nitrate, Atmos. Chem. Phys., 22, 273-293, https://doi.org/10.5194/acp-22-273-2022, 2022.

McWhinney, R. D., Zhou, S., and Abbatt, J. P. D.: Naphthalene SOA: redox activity and naphthoquinone gas–particle partitioning, Atmos. Chem. Phys., 13, 9731-9744, https://doi.org/10.5194/acp-13-

9731-2013, 2013.

Misovich, M. V., Hettiyadura, A. P. S., Jiang, W. Q., and Zhang, Q. Molecular-level study of the photo-oxidation of aqueous-phase guaiacyl acetone in the presence of $^3C^*$: formation of brown carbon products, ACS Earth Space Chem., 5, 1983-1996, https://doi.org/10.1021/acsearthspacechem.1c00103, 2021.

Mladenov, N, Alados-Arboledas, L., Olmo, F .J., Lyamani, H., Delgado, A., Molina, A., and Reche, I.: Applications of optical spectroscopy and stable isotope analyses to organic aerosol source discrimination in an urban area, Atmos. Environ., 45, 1960-1969, https://doi.org/ 10.1016/j.atmosenv.2011.01.029, 2011.

Nau, W. M., and Scaiano, J. C.: Oxygen quenching of excited aliphatic ketones and diketones, J. Phys. Chem., 100, 11360-11367, https://doi.org/10.1021/jp960932i, 1996.

Ng, N. L., Canagaratna, M. R., Zhang, Q., Jimenez, J. L., Tian, J., Ulbrich, I. M., Kroll, J. H., Docherty, K. S., Chhabra, P. S., Bahreini, R., Murphy, S. M., Seinfeld, J. H., Hildebrandt, L., Donahue, N. M., DeCarlo, P. F., Lanz, V. A., Prevot, A. S. H., Dinar, E., Rudich, Y., and Worsnop, D. R.: Organic aerosol components observed in Northern Hemispheric datasets from aerosol mass spectrometry, Atmos. Chem. Phys., 10, 4625-4641, https://doi.org/10.5194/acp-10-4625-2010, 2010.

Onasch, T. B., Trimborn, A., Fortner, E. C., Jayne, J. T., Kok, G. L., Williams, L. R., Davidovits, P., and Worsnop, D. R. Soot particle aerosol mass spectrometer: Development, validation, and initial application. Aerosol Sci. Tech., 46, 804-817, http://dx.doi.org/10.1080/02786826.2012.663948, 2012.

Ou, Y., Nie, D., Chen, H., Ye, Z., Ge, X.: Characterization of products from the aqueous-phase photochemical oxidation of benzene-diols. Atmosphere, 12, 534, https://doi.org/10.3390/atmos12050534, 2021.

Pan, Y., Ma, H., Li, Z., Du, Y., Liu, Y., Yang, J., and Li, G.: Selective conversion of lignin model veratryl alcohol by photosynthetic pigment via photo-generated reactive oxygen species, Chem. Eng. J., 393, 124772, https://doi.org/10.1016/j.cej.2020.124772, 2020.

Raja, P., Bozzi, A., Mansilla, H., and Kiwi, J.: Evidence for superoxide-radical anion, singlet oxygen and OH-radical intervention during the degradation of the lignin model compound (3-methoxy-4-hydroxyphenylmethylcarbinol), J. Photochem. Photobiol. Chem., 169, 271-278,

https://doi.org/10.1016/j.jphotochem.2004.07.009, 2005.

Richards-Henderson, N. K., Hansel, A. K., Valsaraj, K. T., and Anastasio, C. Aqueous oxidation of green leaf volatiles by hydroxyl radical as a source of SOA: Kinetics and SOA yields, Atmos. Environ., 95, 105-112, http://dx.doi.org/10.1016/j.atmosenv.2014.06.026, 2014.

Rossignol, S., Aregahegn, K. Z., Tinel, L., Fine, L., Nozière, B., and George, C.: Glyoxal induced atmospheric photosensitized chemistry leading to organic aerosol growth, Environ. Sci. Technol., 48, 3218-3227, https://doi.org/10.1021/es405581g, 2014.

Scharko, N. K., Berke, A. E., and Raff, J. D.: Release of nitrous acid and nitrogen dioxide from nitrate photolysis in acidic aqueous solutions, Environ. Sci. Technol., 48, 11991-2001, https://doi.org/10.1021/es503088x, 2014.

Salma, I., and Láng, G. G. How many carboxyl groups does an average molecule of humic-like substances contain? Atmos. Chem. Phys., 8, 5997-6002, https://doi.org/10.5194/acpd-8-10005-2008, 2008.

Schauer, J. J., Kleeman, M. J., Cass, G. R., and Simoneit, B. R.: Measurement of emissions from air pollution sources. 3. C1-C29 organic compounds from fireplace combustion of wood, Environ. Sci. Technol., 35, 1716-1728, https://doi.org/10.1021/es001331e, 2001.

Simpson, C.D., Paulsen, M., Dills, R. L., Liu, L.-J.S., and Kalman, A.A. Determination of methoxyphenols in ambient atmospheric particulate matter: Tracers for wood combustion, Environ. Sci. Technol., 39, 631-637, https://doi.org/10.1021/es0486871, 2005.

Smith, J. D., Kinney, H., and Anastasio, C.: Aqueous benzene-diols react with an organic triplet excited state and hydroxyl radical to form secondary organic aerosol. Phys. Chem. Chem. Phys., 17, 10227, https://doi.10.1039/c4cp06095d, 2015.

Smith, J. D., Kinney, H, and Anastasio, C.: Phenolic carbonyls undergo rapid aqueous photodegradation to form low-volatility, light-absorbing products, Atmos. Environ., 126, 36-44, https://doi.org/10.1016/j.atmosenv.2015.11.035, 2016.

Smith, J. D., Sio, V., Yu, L., Zhang, Q., and Anastasio, C.: Secondary organic aerosol production from aqueous reactions of atmospheric phenols with an organic triplet excited state, Environ. Sci. Technol., 48, 1049-1057, https://doi.org/10.1021/es4045715, 2014.

Stephen E. Stein (2014), NIST/EPA/NIH Mass Spectral Library with Search Program - SRD 1a, National Institute of Standards and Technology, https://doi.org/10.18434/T4H594 (Accessed 2022-04-29)

Sun, Y., Zhang, Q., Anastasio, C., and Sun, J.: Insights into secondary organic aerosol formed via aqueous-phase reactions of phenolic compounds based on high resolution mass spectrometry, Atmos. Chem. Phys., 10, 4809–4822, https://doi.org/10.5194/acp-10-4809-2010, 2010.

Tang, S., Li, F., Tsona, N.T., Lu, C., Wang, X., and Du, L.: Aqueous-phase photooxidation of vanillic acid: a potential source of humic-like substances (HULIS), ACS Earth Space Chem., 4, 862-872, https://doi.org/10.1021/acsearthspacechem.0c00070, 2020.

Tsui, W. G., and McNeill, V. F. Modeling secondary organic aerosol production from photosensitized humic-like substances (HULIS), Environ. Sci. Technol. Lett., 5, 255-259. https://doi.org/10.1021/acs.estlett.8b00101, 2018.

Verma, V., Fang, T., Xu, L., Peltier, R. E., Russell, A. G., Ng, N. L., and Weber, R. J.: Organic aerosols associated with the generation of reactive oxygen species (ROS) by water-soluble $PM_{2.5}$, Environ. Sci. Technol., 49, 4646-56, https://doi.org/10.1021/es505577w, 2015a.

Verma, V., Wang, Y., El-Afifi, R., Fang, T., Rowland, J., Russell, A.G., and Weber, R. J.: Fractionating ambient humic-like substances (HULIS) for their reactive oxygen species activity-assessing the importance of quinones and atmospheric aging, Atmos. Environ., 120, 351-359, https://doi.org/10.1016/j.atmosenv.2015.09.010, 2015b.

Vione, D., Albinet, A., Barsotti, F., Mekic, M., Jiang, B., Minero, C., Brigante, M., and Gligorovski, S.: Formation of substances with humic-like fluorescence properties, upon photoinduced oligomerization of typical phenolic compounds emitted by biomass burning, Atmos. Environ., 206, 197-207, https://doi.org/10.1016/j.atmosenv.2019.03.005, 2019.

Vione, D., Maurino, V., Minero, C., Pelizzetti, E., Harrison, M. A., Olariu, R. I., and Arsene, C.: Photochemical reactions in the tropospheric aqueous phase and on particulate matter, Chem. Soc. Rev., 35, 441-53, https://doi.org/10.1039/b510796m, 2006.

Vione, D., Maurino, V., and Minero, C.: Photosensitised humic-like substances (HULIS) formation processes of atmospheric significance: a review, Environ. Sci. Pollut. Res., 21, 11614-11622, https://doi.org/10.1007/s11356-013-2319-0, 2014.

Wang, J., and Wang, S. Reactive species in advanced oxidation processes: Formation, identification and reaction mechanism, Chem. Eng.J., 401, 126158, https://doi.org/10.1016/j.cej.2020.126158, 2020.

Wang, J., Ye, J., Zhang, Q., Zhao, J., Wu, Y., Li, J., Liu, D., Li, W., Zhang, Y., Wu, C., Xie, C., Qin, Y.,

Lei, Y., Huang, X., Guo, J., Liu, P., Fu, P., Li, Y., Lee, H. C., Choi, H., Zhang, J., Liao, H., Chen, M., Sun, Y., Ge, X., Martin, S. T., and Jacob, D .J.: Aqueous production of secondary organic aerosol from fossil-fuel emissions in winter Beijing haze. Proc. Natl. Acad. Sci. USA., 118, e2022179118, https://doi.org/10.1073/pnas.2022179118, 2021.

Wang, L., Lan, X., Peng, W., and Wang, Z.: Uncertainty and misinterpretation over identification, quantification and transformation of reactive species generated in catalytic oxidation processes: A review, J Hazard. Mater., 408, 124436, https://doi.org/10.1016/j.jhazmat.2020.124436, 2021.

Wu, G., Ram, K., Fu, P., Wang, W., Zhang, Y., Liu, X., Stone, E. A., Pradhan, B. B., Dangol, P. M., Panday, A., Wan, X., Bai, Z., Kang, S., Zhang, Q., and Cong, Z.: Water-soluble brown carbon in atmospheric aerosols from Godavari (Nepal), a regional representative of south Asia, Environ. Sci. Technol., 53, 3471-3479, https://doi.org/10.1021/acs.est.9b00596, 2019.

Xie, M., Mladenov, N., Williams, M. W., Neff, J. C., Wasswa, J., and Hannigan, M. P.: Water soluble organic aerosols in the Colorado Rocky Mountains, USA: composition, sources and optical properties, Sci. Rep., 6, https://doi.org/10.1038/srep39339, 2016.

Xu, X., Lu, X., Li, X., Liu, Y., Wang, X., Chen, H., Chen, J., Yang, X., Fu, T., Zhao, Q., and Fu, Q. ROS-generation potential of Humic-like substances (HULIS) in ambient $PM_{2.5}$ in urban Shanghai: Association with HULIS concentration and light absorbance, Chemosphere, 256, 127050, https://doi.org/10.1016/j.chemosphere.2020.127050 0045-6535, 2020.

Yang, J., Au, W. C., Law, H., Lam, C. H., and Nah, T.: Formation and evolution of brown carbon during aqueous-phase nitrate-mediated photooxidation of guaiacol and 5-nitroguaiacol, Atmos. Environ., 254, 118401, https://doi.org/10.1016/j.atmosenv.2021.118401, 2021.

Ye, Z., Zhuang, Y., Chen, Y., Zhao, Z., Ma, S., Huang, H., Chen, Y., and Ge, X.: Aqueous-phase oxidation of three phenolic compounds by hydroxyl radical: Insight into secondary organic aerosol formation yields, mechanisms, products and optical properties, Atmos. Environ., 223, 117240, https://doi.org/10.1016/j.atmosenv.2019.117240, 2020.

Yu, L., Smith, J., Laskin, A., Anastasio, C., Laskin, J., and Zhang, Q.: Chemical characterization of SOA formed from aqueous-phase reactions of phenols with the triplet excited state of carbonyl and hydroxyl radical, Atmos. Chem. Phys., 14, 13801–13816, https://doi.org/10.5194/acp-14-13801-2014, 2014.

Yu, L., Smith, J., Laskin, A., George, K. M., Anastasio, C., Laskin, J., Dillner, A. M., and Zhang, Q.:

Molecular transformations of phenolic SOA during photochemical aging in the aqueous phase: competition among oligomerization, functionalization, and fragmentation, Atmos. Chem. Phys., 16, 4511-4527, https://doi.org/10.5194/acp-16-4511-2016, 2016.

Zhang, T., Huang, S., Wang, D., Sun, J., Zhang, Q., Xu, H., Ho, S., Cao, J., and Shen, Z. Seasonal and diurnal variation of $PM_{2.5}$ HULIS over Xi'an in Northwest China: Optical properties, chemical functional group, and relationship with reactive oxygen species (ROS), Atmos. Environ., 268, 118782, https://doi.org/10.1016/j.atmosenv.2021.118782, 2022.

Zhang, X., Chen, Z. M., and Zhao, Y.: Laboratory simulation for the aqueous OH-oxidation of methyl vinyl ketone and methacrolein: significance to the in-cloud SOA production, Atmos. Chem. Phys., 10, 9551-9561, https://doi.org/10.5194/acp-10-9551-2010, 2010.

Zhao, R., Lee, A. K., and Abbatt, J. P.: Investigation of aqueous-phase photooxidation of glyoxal and methylglyoxal by aerosol chemical ionization mass spectrometry: observation of hydroxyhydroperoxide formation, J. Phys. Chem. A., 116, 6253-63, https://doi.org/10.1021/jp211528d, 2012.

Zhao, R., Mungall, E. L., Lee, A. K. Y., Aljawhary, D., and Abbatt, J. P. D.: Aqueous-phase photooxidation of levoglucosan-a mechanistic study using aerosol time of flight chemical ionization mass spectrometry (Aerosol ToF-CIMS), Atmos. Chem. Phys., 14, 9695-9706, https://doi.org/10.5194/acpd-14-8819-2014, 2014.

Zhao, R., Lee, A.K.Y., Huang, L., Li, X., Yang, F., and Abbat, J.P.D.Photochemical processing of aqueous atmospheric brown carbon, Atmos. Chem. Phys., 15, 6087-6100, https://doi.org/10.5194/acpd-15-2957-2015, 2015.

Zhou, Z., Chen, B., Qu, X., Fu, H., and Zhu, D.: Dissolved black carbon as an efficient sensitizer in the photochemical transformation of 17#-estradiol in aqueous solution, Environ. Sci. Technol., 52, 10391-10399, https://doi.org/10.1021/acs.est.8b01928, 2018.